

1

NOvA Test Beam detector calibration

2

Technical Note

3

Róbert Králik

University of Sussex

4

October 3, 2023

5

Abstract

6

The NOvA Test Beam detector calibration uses the same calibration procedure as the
7 standard NOvA detectors. The main aim is to remove differences in energy deposition
8 within the detector and to provide an absolute energy scale from collected charge to phys-
9 ical energy units. This allows for a direct comparison of the deposited energy in the Test
10 Beam detector with the standard NOvA detectors. On top of that, the unique qualities of
11 Test Beam allow us to use the Test Beam calibration to validate the calibration process and
12 possibly to provide a simulation-independent absolute energy scale.

13 Contents

14	1	Introduction	3
15	2	Overview of the Test Beam detector	3
16	3	NOvA calibration process	7
17	3.1	Relative calibration	12
18	3.2	Absolute calibration	13
19	3.3	Calibration uncertainties	13
20	4	NOvA Test Beam detector calibration	14
21	4.1	Fibre Brightness	15
22	4.2	Threshold and shielding corrections	15
23	4.3	Simulation	17
24	4.4	Period 1 data	17
25	4.5	Period 2 data	20
26	4.6	Period 3 data	26
27	4.7	Period 4 data	32
28	4.8	Absolute calibration results	36
29	4.9	Results	36
30	4.10	Validation	36
31	5	Conclusion	51

32 1 Introduction

33 The NOvA Test Beam experiment aims to improve NOvA's sensitivity to the neutrino oscillation
34 parameters by improving our understanding of particle interactions and energy deposition
35 in the NOvA detectors, with the hope of reducing the total systematic uncertainty by about 10%
36 [?].

37 Specifically, Test Beam allows us to study the response of tagged single particles as a function
38 of their measured energies and compare it to the simulated prediction. It also enables us to
39 determine the energy resolution and the absolute energy scale of these particles. Additionally,
40 we are able to compare the response of beam and cosmic ray muons, to study fibre attenuation,
41 or to validate the entire NOvA calibration process. Test Beam detector was also equipped with
42 a combination of near and far detector readout electronics and filled with a variety of NOvA
43 scintillator oils, which makes it possible to make a comparison of their responses [?].

44 All the aforementioned benefits of running the NOvA Test Beam experiment require, or
45 benefit from, the Test Beam detector calibration.

46 The Test Beam detector calibration was first pioneered by Kevin Moulder who adapted the
47 NOvA calibration codebase for Test Beam and tested it on period 1 Test Beam data [?]. This
48 was followed by Anna Hall who improved it and got the first usable calibration of the Test
49 Beam detector based on the period 2 data [?]. Lastly, Rober Kralik took over and finished the
50 Test Beam calibration with all Test Beam data and a new simulation in 2023 [?].

51 2 Overview of the Test Beam detector

52 The NOvA Test Beam detector is a scaled down version of the near and far detectors shown on
53 figure 1. It is placed in the MC7b enclosure of the Fermilab Test Beam Facility in the path of
54 the MCcenter beamline with a variety of beamline detectors to measure and identify a range of
55 particles with various momenta [?].

56 The Test Beam detector started with commissioning runs in May 2019 and ran, with an
57 exception of regular summer shutdowns, until July 2022, after which it was decommissioned.
The Test Beam data periods are:

Period 1	March 22 nd 2019	- July 6 th 2019
Period 2	December 5 th 2019	- March 20 th 2020
Period 3	January 12 th 2021	- June 27 th 2021
Period 4	November 30 th 2021	- July 10 th 2022

Table 1: Test Beam detector data taking periods.

58
59 Majority of the Test Beam detector and its instrumentation is identical to the other NOvA
60 detectors, with a few exceptions that could have an impact on the calibration. We are going to
61 identify and discuss these differences in this section.

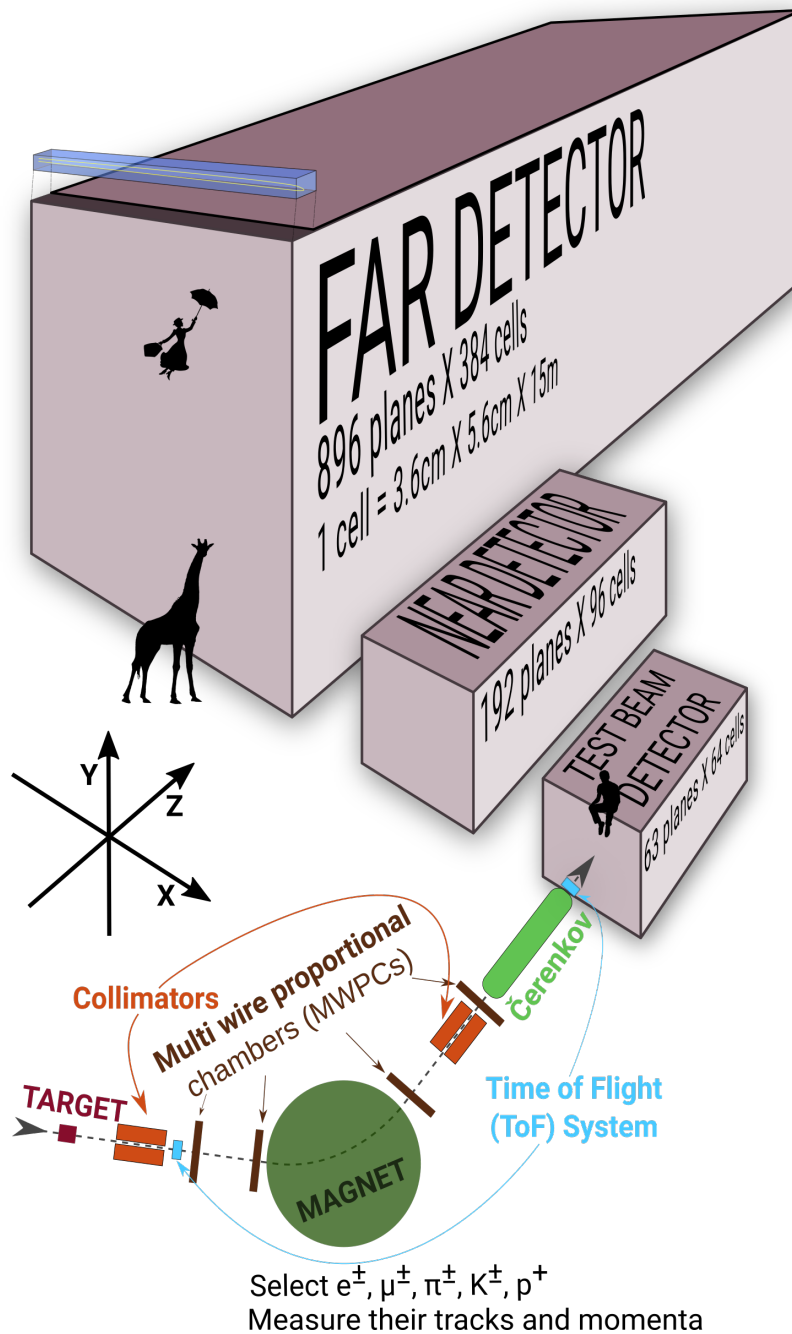


Figure 1: Comparison of Test Beam detector scale to the Near and Far NOvA detectors (and a man, giraffe, or Mary Poppins). Also shown are the Test Beam beamline detectors and components (not to scale), with arrows showing the direction of the beam. The three black arrows show the orientation of the detector coordinate system.

62 General parameters

- 63 The NOvA Test Beam detector consists of two 31-plane blocks, each beginning and ending
 64 with a vertical plane, with an additional horizontal plane glued in-between them to preserve
 65 the alternating pattern [?]. Each plane consists of 2 modules side-by-side, both made up of 32

66 cells. Each cell is 2.6 m long with an inner (without the PVC) depth and width of 5.9 cm and
67 3.8 cm respectively, same as for the other NOvA detectors. This brings the final dimensions of
68 the Test Beam detector to 63 planes \times 64 cells, or $2.6 \times 2.6 \times 4.1 \text{ m}^3$.

69 The 63 planes are numbered from 0 to 62, with even numbers corresponding to vertical
70 planes and odd numbers to horizontal planes. Cells are numbered 0 to 63, going from bottom
71 to top for horizontal planes and left to right, when facing the front of the detector, for vertical
72 planes.

73 The detector coordinate system is illustrated on figure 1. It is centred with (0,0,0) in the
74 centre of the first plane [?]. The x axis runs left to right when facing the front of the detector,
75 y axis bottom to top, and z axis goes along the beam direction from front to the back of the
76 detector. Position within each cell (w) is aligned with the x (y) axis for the horizontal (vertical)
77 cells, with $w = 0$ centred in the middle of each cell. The exact geometry of the Test Beam
78 detector was measured in several alignment surveys and is saved in gdml files [?].

79 In the past we encountered an issue when trying to align the Test Beam detector with the
80 beamline measurements by rotating the detector. This broke several assumptions within the
81 Test Beam geometry [?] and manifested as uncalibrated cells in the back of the detector [?].
82 This was fixed by realigning both the detector and the beamline separately, based on the last
83 alignment survey, measured during the decommissioning of the detector. We implemented the
84 fix in the production tag R23-04-05-testbeam-production.a [?].

85 Scintillator

86 Test Beam used a combination of the leftover near and far detector production scintillator oils
87 and the oil drained from the NDOS test detector. The used scintillator oils also differ in the
88 way they were stored since the filling of the near and far detectors, or NDOS draining, which
89 apparently impacted its quality. The distribution of individual scintillator oils and the relative
90 difference in their energy response can be seen on figure 2.

91 We can distinguish four samples of the NOvA scintillator oil used in the Test Beam detector:

- 92 • Mixed near detector production oil and NDOS-drained oil stored in a tanker and tanks
93 outside in Fermilab [?];
- 94 • Separate near detector production oil and NDOS-drained oil stored underground in barells
95 at MiniBooNE [?];
- 96 • Far detector production oil stored inside in Ash River in "totes" under several layers of
97 black plastic [?];
- 98 • NDOS-drained oil stored mainly inside at Texas A&M University and University of
99 Texas at Austin [?, ?].

100 The original plan [?] was to only use the tanker/tank scintillator (sample 1). First tests
101 showed acceptable results and the tanker oil was used to fill out almost the entirety of the first
102 block of the detector (first 32 planes) [?]. However, when we loaded oil from tank two into
103 the tanker, it became extremely cloudy and unusable, possibly due to contamination with water
104 accumulated at the bottom of the tanks. The rest of the first block was therefore topped up with
105 high quality scintillator from NDOS (sample 2). This is labelled as "Fermilab ND+NDOS oil"
106 on figure 2.

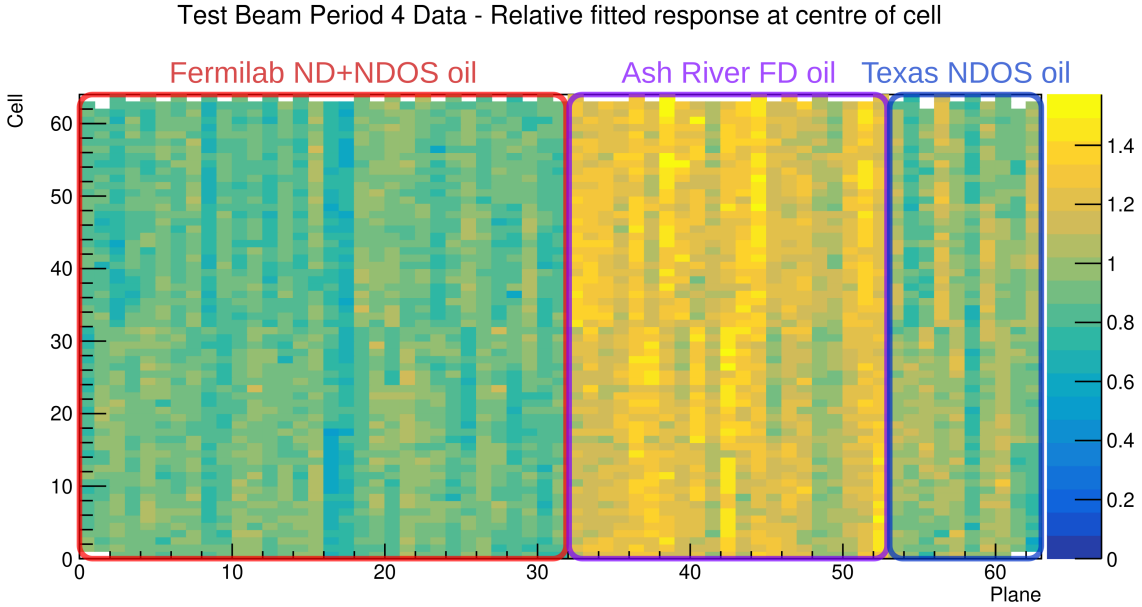


Figure 2: Uncorrected energy response in the centre of cells across the Test Beam detector showing a clear distinction between the different scintillator oils, shown with coloured boxes.

The first 21 planes of the second block (planes 32 to 52) were filled with the far detector production scintillator shipped in from Ash River (sample 3) [?]. We again topped up these planes with the ND+NDOS scintillator (sample 2) [?].

The last 10 planes (planes 53 to 62) [?] were filled with the "Texas" scintillator (sample 4), which has higher light yield than the one from the tanker, but lower than the Ash River one [?].

In total the Test Beam detector is filled with 5418 gallons of scintillator oil with a weight of approximately 28.6 tons [?].

114 **Readout**

The Test Beam detector uses in total 126 Front End Boards (FEBs), each reading out signal from 32 cells (one module = half of a plane) [?]. The readout is located on the top and right side (when looking at the front) of the detector. 118 FEBs are version 4.1, same as in the Far Detector, and 8 FEBs, located in pairs on planes 16, 17, 48 and 49, are version 5.2, same as in the Near Detector. The Near Detector FEBs are designed to read out data in a faster rate and we used a mix of FEB types to study the difference in their response and to validate both versions in the same environment [?].

122 **Environment**

Unlike the near and the far detector, the Test Beam detector does not have any overburden to shield it from cosmic particles, which affects their rate and energies inside the detector. There is also less precise control of temperature and humidity than in the other detectors [source?], which can potentially impact the scintillator and readout performance.

127 **Underfilled cells issue**

128 The Test Beam detector is slightly tilted around the Z axis by about 0.7° towards the readout.
129 This caused the top cells of both modules of all the horizontal planes (cells 31 and 63) to be
130 underfilled, creating an air bubble on the left side of the detector and severely affecting the
131 energy response in those cells [?]. This has been fixed [?] during the period 3 running by
132 adding extensions to the filling ports and overfilling the horizontal cells with the ND+NDOS
133 scintillator (sample 2).

134 **3 NOvA calibration process**

135 Test Beam is following the same ideas and procedures as the standard NOvA calibration. This
136 section intends to provide only a brief overview of the NOvA calibration, with further details
137 in the range of NOvA calibration technical notes [?]. All the code required for calibration is
138 located in the NOvASoft Calibration package and the outline of the files and processes in
139 NOvA calibration are shown on figure 3.

140 The purpose of calibration is to make sure that we get the same amount of energy wherever
141 or whenever it's deposited in whichever of NOvA's detectors and to express this amount of
142 energy in physical units. The NOvA calibration uses cosmic ray muons, which provide a
143 consistent, abundant, and well-understood source of energy deposition and consists of two
144 parts [?]:

- 145 1. The **relative calibration** corrects for attenuation of scintillator light as it travels through
146 the cell to the readout, as well as for differences between detector cells. This correction
147 is calculated for each cell separately.
- 148 2. Followed by the **absolute calibration**, which only uses stopping muons when they are
149 minimum ionising particles. In the absolute calibration we calculate a scale between
150 the measured energy deposition, corrected by the relative calibration, and the simulated
151 energy deposition in physical units of MeV. This scale is calculated for each time period
152 and each detector separately, which ensures the energy deposition is directly comparable
153 wherever or whenever it occurred.

154 The NOvA calibration process technically also involves **timing calibration**, which corrects
155 for the time differences of the signal to be processed [?]. However, this is done as a separate
156 project to the relative and absolute calibrations and is out of scope of this technical note.

157 The basic units and variables used to define energy deposited in the NOvA detectors are
158 listed in table 2.

The final result of the NOvA calibration is the deposited energy in terms of physical units,

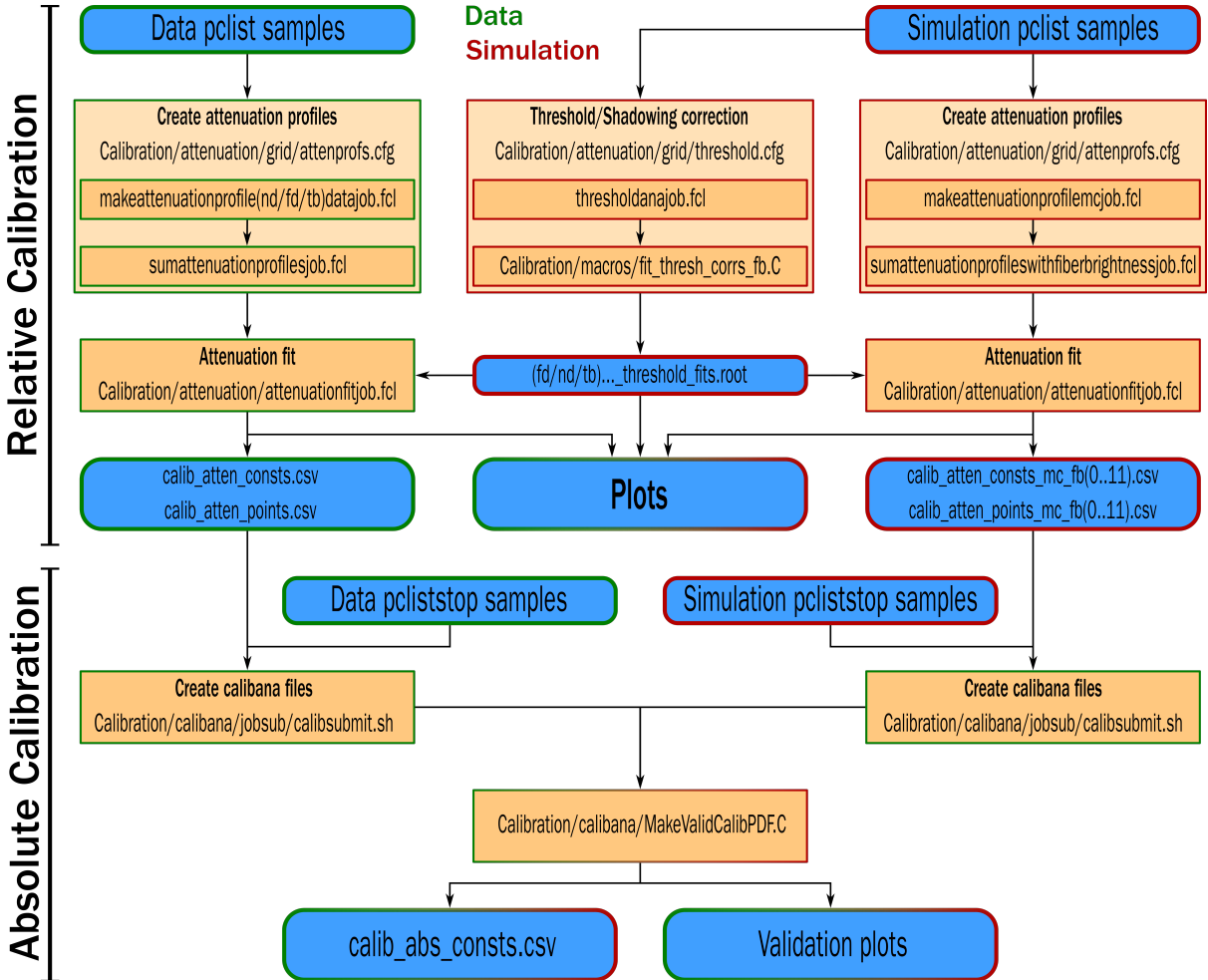


Figure 3: Flow chart showing the jobs (orange background) and files (blue background) needed and produced during the full NOvA calibration process. The left chain is showing the data calibration process (with green border) and is applied to every data calibration sample separately (periods or epochs). The center and right chains are showing the simulation calibration process (red border), which is redone only if there's a change to the detector simulation. The absolute calibration at the bottom combines data and simulation. The entire process is done separately for each NOvA detector.

ADC	The digitized charge collected by the APDs from the Analog to Digital Converter [?].
PE	Number of Photo Electrons. Calculated by a simple rescaling of the best estimate of the peak ADC. The PE per ADC scale only depends on the FEB type and the APD gain settings. This conversion is done before the calibration and PE serves as the base unit for calibration.
PECorr	Corrected PE after applying the relative calibration results. The correction is a ratio between an average energy response (a pre-determined semi-arbitrary number) and the result of the the relative calibration fit (also called attenuation fit), which depends on w, cell, plane, epoch and detector. This makes the energy response equivalent across each detector.
MEU	Muon Energy Unit is the mean detector response to a stopping cosmic minimum ionising muon. For true variables it's equivalent to the mean MeV/cm and for reconstructed variables to the mean PECorr/cm.
MeV	Estimated energy deposited in the scintillator calculated from PECorr using the results of the absolute calibration. Additional correction for dead material needs to be made in order to get an estimate of the calorimetric energy.

Table 2: Definitions of variables commonly used in calibration [?, ?].

which is in effect calculated as:

$$E_{dep}[\text{MeV}] = \underbrace{\frac{\text{MEU}_{truth}[\text{MeV}/\text{cm}]}{\text{MEU}_{reco}[\text{PECorr}/\text{cm}]}}_{\substack{\text{Absolute calibration} \\ (\text{Detector, epoch})}} \times \underbrace{\frac{\text{Average response}[PECorr]}{\text{Fitted response}[PE]}}_{\substack{\text{Relative calibration} \\ (\text{Detector, epoch, plane, cell, w})}} \times \underbrace{\left[\frac{\text{PE}}{\text{ADC}} \right]}_{\substack{\text{Scale} \\ (\text{APD Gain, FEB})}} \times \text{Signal}[\text{ADC}], \quad (1)$$

where both the relative calibration results (blue fraction) and the absolute calibration results (red fraction) are stored in a database and applied together with the ADC-to-PE scale by the NOvASoft Calibrator package during processing of every hit in the NOvA detectors.

162 Creating calibration samples

163 We want to select good quality cosmic ray muons. First, we remove beam related events based
 164 on their time stamps relative to the time of the beam spill, using the RemoveBeamSpills (for
 165 the near and far detectors), or RemoveTBSpills filter (for the Test Beam detector), as shown
 166 on figure 4. Next we apply reconstruction to get the CellHit, slicer, and track information,
 167 followed by a track-based selection to remove misreconstructed and poor quality events.

168 Since energy deposition depends on the path length particle travels through a cell, we only
 169 use hits for which we can reliably calculate their path length. We call these hits **tricell** hits, as
 170 we require that all accepted hits are accompanied by a recorded hit in both neighbouring cells
 171 of the same plane, as shown on figure 5. In case there is a bad channel in a neighbouring cell,

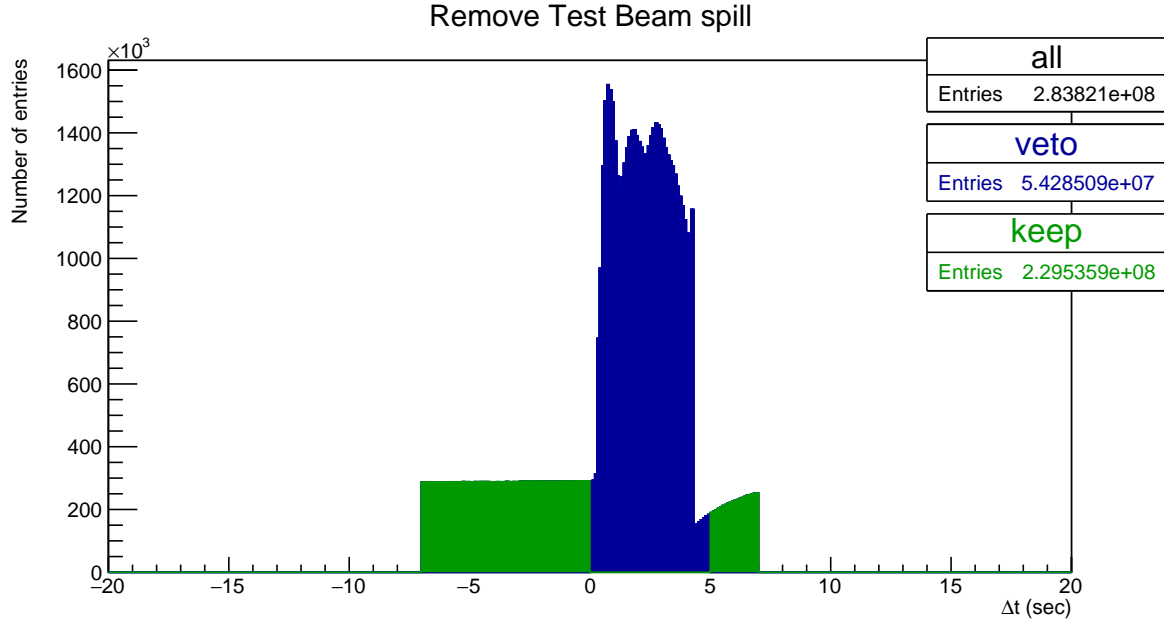


Figure 4: Test Beam beam spill events removed from the calibration samples. Test Beam beam spill is 4.2 seconds long and we remove events (in blue) within a 5 seconds window from the start of the beam spill. The remaining events (green) should mostly consist of cosmic particles. This example and the numbers of entries are for the full period 4 Test Beam sample.

¹⁷² we ignore this channel and look one cell further. We can then calculate the path length simply
¹⁷³ as the cell width divided by the cosine of the direction angle [?, ?].

¹⁷⁴ For the absolute calibration we select muons that stop inside the detector, by identifying
¹⁷⁵ muons with a Michel electron at the end of their track [?].

¹⁷⁶ For each data period or epoch and for each version of the simulation we create two calibra-
¹⁷⁷ tion samples that are used as the input for the relative and absolute calibration. The samples
¹⁷⁸ are called [?]

- ¹⁷⁹ • pclist = **list** of pre-calibrated hist; Contains all selected cosmic muon events and is used
¹⁸⁰ in the relative calibration;
- ¹⁸¹ • pcliststop = pclist files only containing stopping muons used for the absolute calibration

¹⁸² Fibre brightness

¹⁸³ For data, the relative calibration is done for each individual cell in each plane to properly
¹⁸⁴ account for any potential variations, repeating the attenuation fit $N_{cell} \times N_{plane}$ times. However,
¹⁸⁵ generating enough simulated events turned out to be computationally expensive. Therefore,
¹⁸⁶ assuming the simulated detector is approximately uniform plane to plane, for simulation we
¹⁸⁷ can "consolidate" the detector planes and only consider variations in the two views. Therefore
¹⁸⁸ for simulation we would repeat the fit $N_{cell} \times N_{view}$ times [?, ?].

¹⁸⁹ However, there are some variations in the detector response cell by cell that can be caused
¹⁹⁰ by different fibre brightnesses, but also by different qualities of the scintillator, air bubbles,
¹⁹¹ APD gains, looped or zipped fibres and potentially others. We want to include these variations

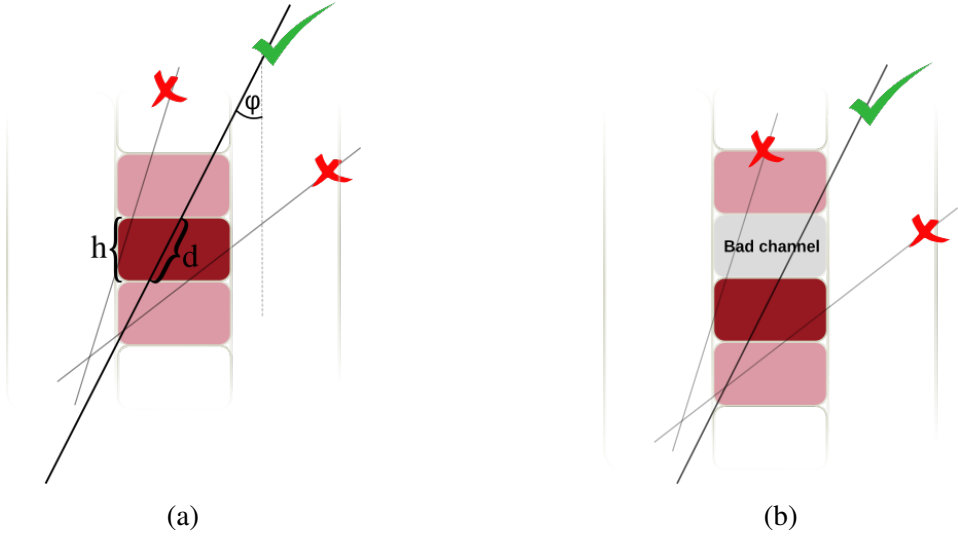


Figure 5: Illustration of the tricell condition (a). We only use hits that have two surrounding hits in the same plane to be used in the NOvA calibration. This is to ensure a good quality of the path length (d) reconstruction, which is calculated from the known cell height (h) and the reconstructed track angle (φ). In case the hit is next to a bad channel (b), we ignore this bad channel and require a hit in the next cell over.

in the simulation to better match data. To emulate these differences in the simulation without the need to simulate every cell individually, we divide each detector into 12 brightness bins, as shown on figure 6. These brightness bins describe the relative differences in the detector response between individual cells [?]. Therefore in the end, for simulation we perform the attenuation fit $N_{cell} \times N_{view} \times N_{BrightnessBin}$ times.

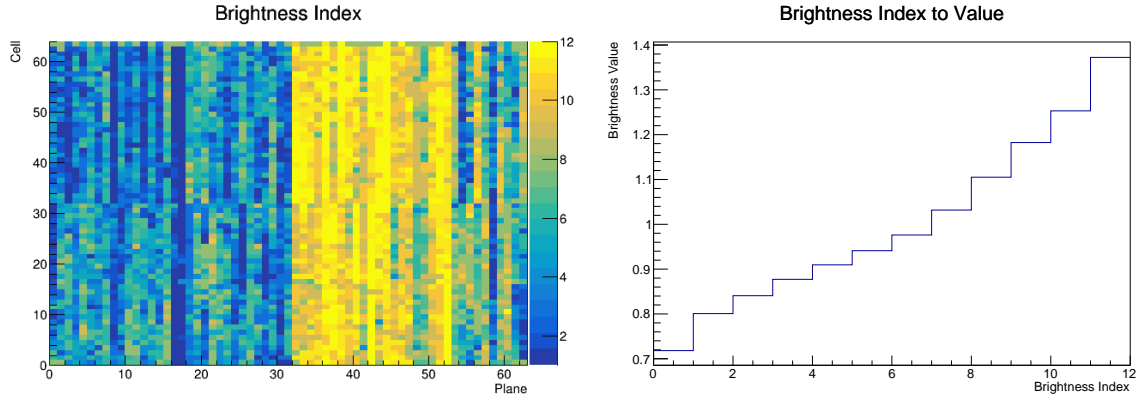


Figure 6: The Test Beam detector is (like the standard NOvA detectors) divided into 12 brightness bins (left plot), each representing a relative difference in energy response (right plot) due to different brightnesses of the fibres, scintillators, or readout.

To divide each detector into the 12 brightness bins, we use results from the relative calibration. Specifically we take the result of the attenuation fit (equal to the average response) in the centre of each cell to fill a 2D histogram. Then we normalize this histogram by dividing the response in each Cell \times View \times Plane by the average response in the corresponding

201 Cell \times View. All uncalibrated cells get assigned the average response (1 in normalized his-
202 togram). Then we make a 1D histogram filled with the normalized responses of each cell and
203 divide this histogram into 12 equally populated bins (so each bin represents approximately the
204 same number of detector cells, shown on the left plot of figure 6). The mean normalized re-
205 sponse in each bin represents the relative brightness value of this bin (right plot of figure 6).
206 A ROOT file with the distribution of brightness bins across the detector and their correspond-
207 ing relative brightness values is stored inside the NOvAsoft PhotonTransport package as
208 <det>BrightnessFromCosmics.root.

209 **Threshold and shielding correction**

210 Energy deposited far away from the readout may get attenuated enough to be shifted below the
211 threshold. These low energy depositions would be missing from the attenuation fit, biasing it
212 towards larger light levels with increasing distance from the readout. Similar effect, specifically
213 for the vertical cells, is caused by using cosmic muons for calibration and applying it to beam
214 muons. The top of the detector effectively shields the bottom, skewing the energy distribution
215 of cosmic muons. To correct for both of these effect, we use the simulation plist sample to
216 calculate the threshold and shielding (also called threshold and shadowing) correction by com-
217 paring the true and reconstructed information. We apply this correction before the attenuation
218 fits [?].

219 **3.1 Relative calibration**

220 Relative calibration corrects for the attenuation of the scintillator light by fitting the average
221 detector response over the position in each cell (w), separately for every cell inside each de-
222 tector. Dividing the "average response" of the detector by the result of the attenuation fit for
223 each Plane \times Cell $\times w$ combination effectively removes relative differences within and between
224 all cells across the entire detector. The average response is a single constant number chosen to
225 approximately represent the average response in the middle of the cell. Its value is for the far
226 detector and Test Beam 39.91 PE and for the near detector 37.51 PE. The value of the average
227 response has no impact of the calibration results, as the absolute scale of the detector response
228 is determined during the absolute calibration and relative calibration only serves to remove the
229 relative differences [?, ?].

230 To create the attenuation fit we use the following procedure [?]:

- 231 1. Create the *attenuation profiles*. Attenuation profiles are essentially profile histograms of
232 detector response in terms of PE/cm as a function of position in the cell (w) for each cell
233 in all planes. We construct the attenuation profiles over a little wider range than the actual
234 length of the cell and always with 100 bins for each detector. This means that smaller
235 detectors, like the Test Beam detector, have a finer binning ($\sim 3\text{cm/bin}$) compared to the
236 Far Detector ($\sim 18\text{cm/bin}$).
- 237 2. Analyse the attenuation profiles. The job to create the attenuation profiles also creates
238 validation histograms, which should be analysed prior to performing the attenuation fit
239 to make sure the attenuation profiles look as expected.
- 240 3. Apply the threshold and shielding correction that was created before the relative calibra-
241 tion.

242 4. Do the attenuation fit over the full length of each cell. The fit consists of

- 243 (a) an exponential fit, which combines two cases. First, when the scintillating light
244 travels the short distance straight to the readout, and second, when it goes to the far
245 side of the cell and loops around before going to the readout. The fitted function
246 has a form:

$$y = C + A \left(\exp\left(\frac{w}{X}\right) + \exp\left(-\frac{L+w}{X}\right) \right), \quad (2)$$

247 where y is the fitted response, L is the length of the cell and C, A and X are the fitted
248 parameters. X also represents the attenuation length.

- 249 (b) Smoothing of the residuals from the exponential fit, mainly at the end of cells, with
250 the LOcally WEighted Scatter plot Smoothing (LOWESS) method.

251 5. Check the plots of the attenuation fit for a selection of cells.

252 6. Save the fit result to the database in the form of two csv tables. The `calib_atten_consts.csv`
253 table holds the results of the exponential fit, together with the final χ^2 of the fit. The
254 `calib_atten_points.csv` table holds the results of the LOWESS smoothing.

255 To ensure the quality of the attenuation fit, we only apply the results if the final $\chi^2 < 0.2$.
256 If $\chi^2 > 0.2$, we ignore the results for this cell and mark it as *uncalibrated*.

257 3.2 Absolute calibration

258 To find the absolute energy scale, we apply the relative calibration results on the stopping
259 muon sample and look at the energy they deposited in cells 1-2 meters from the end of their
260 tracks. In this track window they are approximately minimum ionising particles and their
261 energy deposition is almost constant and well understood. Additionally, we don't use hits from
262 the edges of a cell, as those might be affected by the lower number of events and fibre endings,
263 or loops. We take a mean of their corrected deposited energy separate for each view and for
264 each calibrated sample. We then take the average over the two views to get the final MEU_{reco}
265 in PECorr/cm for each sample [?].

266 From simulation we get the mean of the true energy deposited in scintillator MEU_{truth} in
267 MeV/cm for the same sample of stopping muons. We ignore the energy that is lost in the
268 dead material (PVC extrusions) and deal with it separately. The absolute energy scale for each
269 sample is then the ratio of $\text{MEU}_{truth}/\text{MEU}_{reco}$. We save these absolute energy scales in another
270 csv table called `calib_abs_consts.csv` which stores the MEU values and their errors.

271 As part of the absolute calibration we also produce validation plots that show the effect of
272 calibration on the distribution of the stopping muons. We analyse these plots and if everything
273 looks all right we load all the csv tables into the database.

274 3.3 Calibration uncertainties

275 WORK IN PROGRESS

²⁷² 4 NOvA Test Beam detector calibration

²⁷³ In this section we describe the details of the Test Beam detector calibration as it was finalized
²⁷⁴ in June 2023. This version includes all measured Test Beam data, with the exception of Period
²⁷⁵ 1, which was only used for commissioning and is not used in any Test Beam analysis. The
²⁷⁶ specific commands and tips for running the Test Beam detector calibration are listed on the
²⁷⁷ [Test Beam calibration redmine wiki page](#).

²⁷⁸ The calibration samples used for the Test Beam detector calibration are listed in table 3. We
²⁷⁹ are using data from one of the Test Beam data-driven activity-based triggers (DDActivity1).
²⁸⁰ To produce these samples we (or production) use the `prod_tb_ddactivity1_pclist_job.fcl` file
²⁸¹ from the novaprod/novaproduction/fcl/testbeam repository, or the corresponding mc file. The
²⁸² calibration samples were originally created in keep-ups by the production, but most of them
²⁸³ had to be reproduced in 2023 to fix a bug in the Test Beam geometry.

pclist samples

Data period 2:

`prod_pclist_R23-04-05-testbeam-production.a_testbeam_ddactivity1_period2_v1`

Data period 3:

`prod_pclist_R23-04-05-testbeam-production.a_testbeam_ddactivity1_epoch3a_v1`

`prod_pclist_R23-04-05-testbeam-production.a_testbeam_ddactivity1_epoch3b_v1`

`prod_pclist_R23-04-05-testbeam-production.a_testbeam_ddactivity1_epoch3c_v1`

`pclist_testbeam_detector_activity_epoch3d_R21-01-28-testbeam-production.a`

`pclist_testbeam_detector_activity_epoch3e_R21-01-28-testbeam-production.a`

Data period 4:

`prod_pclist_R23-04-05-testbeam-production.a_testbeam_ddactivity1_period4_v1`

Simulation:

`rkrilik_pclist_testbeam_databasedsim_R23-04-05-testbeam-production.a`

pcliststop samples

Data period 2:

`prod_pcliststop_R23-04-05-testbeam-production.a_testbeam_ddactivity1_period2_v1`

Data period 3:

`prod_pcliststop_R23-04-05-testbeam-production.a_testbeam_ddactivity1_epoch3a_v1`

`prod_pcliststop_R23-04-05-testbeam-production.a_testbeam_ddactivity1_epoch3b_v1`

`prod_pcliststop_R23-04-05-testbeam-production.a_testbeam_ddactivity1_epoch3c_v1`

`pcliststop_testbeam_detector_activity_epoch3d_R21-01-28-testbeam-production.a`

`pcliststop_testbeam_detector_activity_epoch3e_R21-01-28-testbeam-production.a`

Data period 4:

`prod_pcliststop_R23-04-05-testbeam-production.a_testbeam_ddactivity1_period4_v1`

Simulation:

`rkrilik_pcliststop_testbeam_databasedsim_R23-04-05-testbeam-production.a`

Table 3: SAMWEB definitions of the Test Beam calibration samples.

284 4.1 Fibre Brightness

285 To divide the Test Beam detector into fibre brightness bins we used the attenuation fit results
 286 for period 4 data (described in section 4.7), since that is the best detector conditions data we
 287 have.

288 As we are only using the attenuation fit results in the centre of each cell, we've decided
 289 to allow some cells that initially failed the calibration, to be still used for the creation of the
 290 brightness file. Otherwise, these cells would be assigned the average response and we would
 291 loose the information on their relative brightness. As can be seen on figure 7, some attenuation
 292 fits have $\chi^2 > 0.2$, even though they correctly represent the energy deposition in the centre of
 293 that cell. By carefully investigating all cells with $\chi^2 > 0.2$ (possible for Test Beam, due to
 294 its small number of cells), we concluded it is safe to use all attenuation fit results, for which
 295 $\chi^2 < 0.7$.

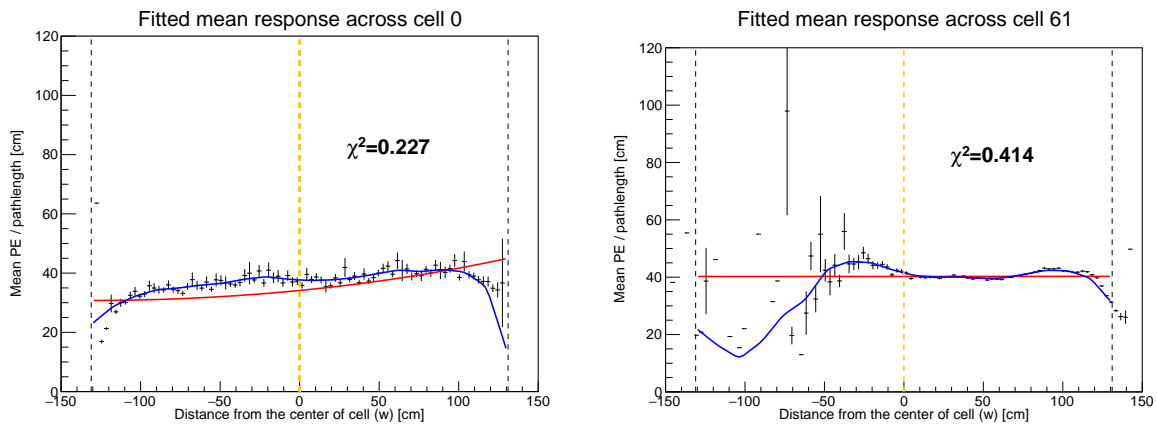


Figure 7: Attenuation fits for two cells that fail the calibration condition, but the fit (blue line) correctly represents the energy deposition in the centre of that cell (yellow dashed line).

296 The final distribution of brightness bins and their corresponding relative brightnesses for
 297 the Test Beam detector is shown on figure 6.

298 4.2 Threshold and shielding corrections

299 We created the threshold and shielding correction for Test Beam from the new simulation de-
 300 scribed in the next section 4.3. As can be seen on figure 8 the correction is almost uniform as
 301 a function of both w and cell number. This is the case for all fibre brightness bins and for both
 302 views. The uniform distribution is expected as the Test Beam detector is much smaller than
 303 the far detector, which motivated creating the correction. The cell length of 2.6 m has only
 304 a negligible effect on the energy distribution of cosmic muons or on the threshold saturation.
 305 Therefore the threshold and shielding correction for Test Beam is only a normalization factor,
 306 except for the cell edges, but there is a large variation in the energy response there anyway due
 307 to low number of events. Since the relative calibration only cares about relative differences
 308 across the detector, a normalization factor does not have any impact on its results.

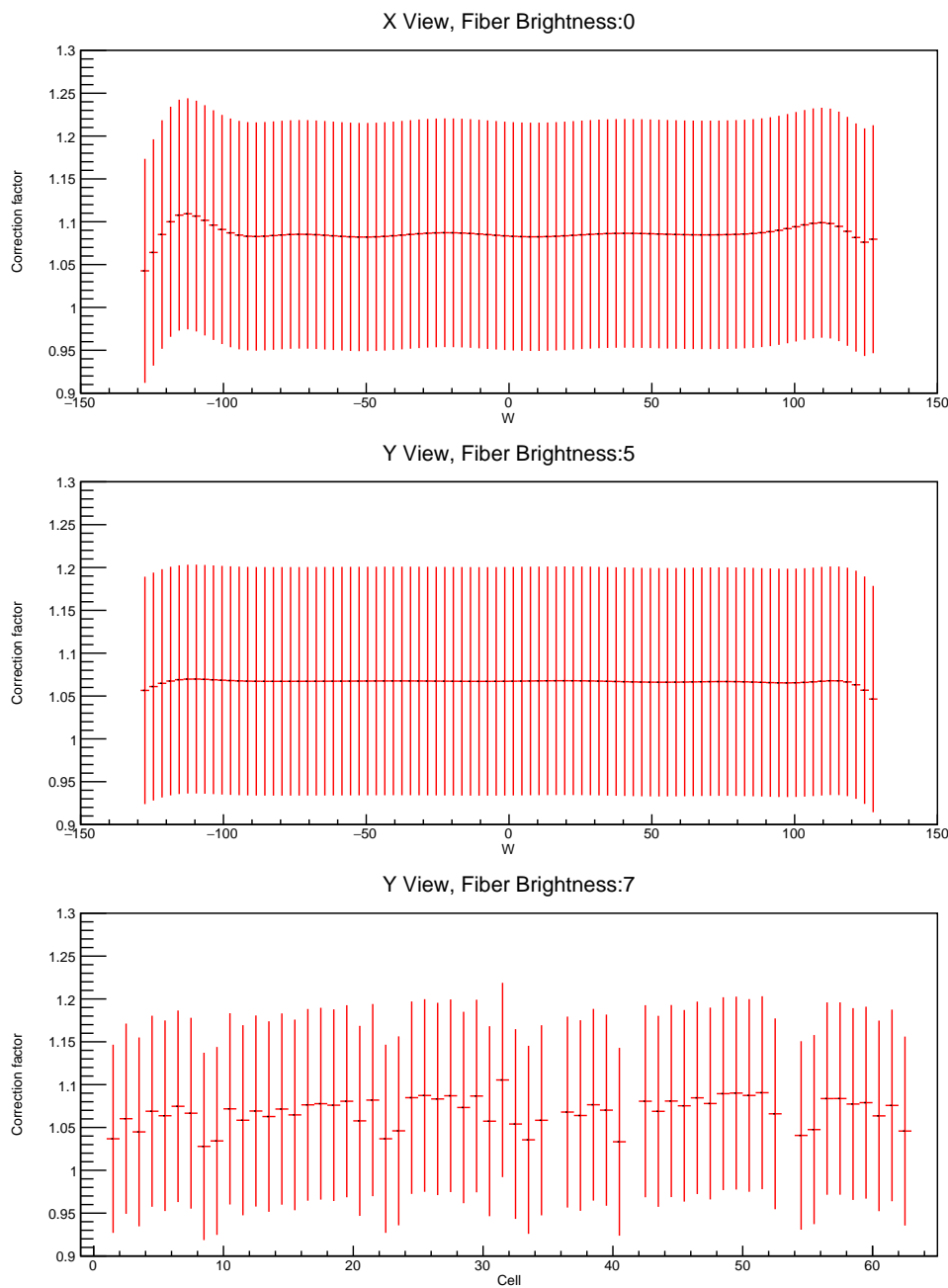


Figure 8: Examples of threshold and shielding corrections for the Test Beam detector

309 **4.3 Simulation**

310 We used a data-based simulation of cosmic muons for the Test Beam detector calibration. The
311 details are described in the Data-based simulation of cosmic muons (not only) for calibration
312 technical note [?]. We used half of period 4 data (used every second event as saved in the root
313 file, therefore sampled from the entire period 4) as inputs and the newly created fibre brightness
314 file to inform the simulation on the realistic detector conditions.

315 The distribution of events cosmic muon events from the new simulation is shown on figure
316 [9](#).

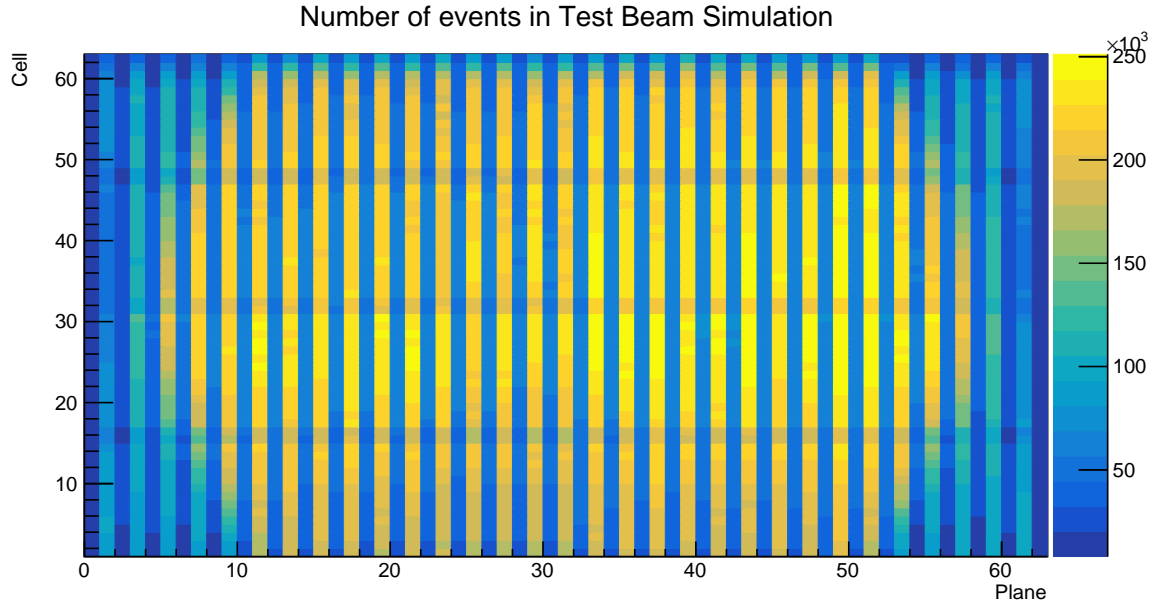


Figure 9: Distribution of events in the Test Beam simulation calibration sample.

317 The results of the attenuation fit are shown for each cell (in its centre) on figure 10. The
318 blank cells show which cells failed the attenuation fit (their $\chi^2 > 0.2$). Most of the uncalibrated
319 cells are on the edges of the detector, which is expected as those have much fewer events than
320 pass our selection than the rest. Examples of a standard detector response and of the response
321 for cells on the edge of the detector are shown of figure 11.

322 (I should explain here what is on the plots maybe - red is the exponential fit and blue is the
323 total with with the LOWESS. Most cells have the expected response of slow rise towards the
324 readout falling down on the edges).

325 There is only one cell in the middle of the detector that is left uncalibrated, which is the cell
326 32 in a vertical plane in the brightness bin 5, shown on the top right of fig.11. The corresponding
327 $\chi^2 = 0.227$. It seems the reason the $\chi^2 > 0.2$ is an exceptionally high response with a large
328 uncertainty in the last bin.

329 This is a much better result of the relative calibration (attenuation fit) for a simulation than
330 the previous versions of Test Beam detector calibration simulations were able to accomplish.

331 **4.4 Period 1 data**

332 TO DO: add a description of period 1 data

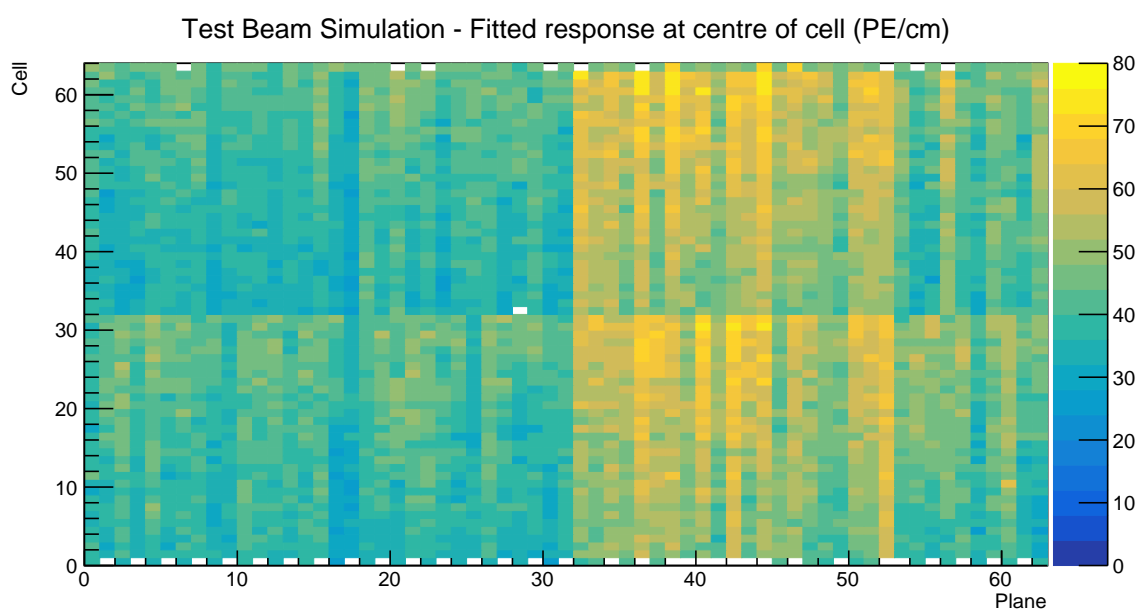


Figure 10: Overview of the attenuation fit results for the Test Beam detector calibration simulation. Each cell represents the result of the attenuation fit to the energy response in the centre of that cell. The blank cells are uncalibrated.

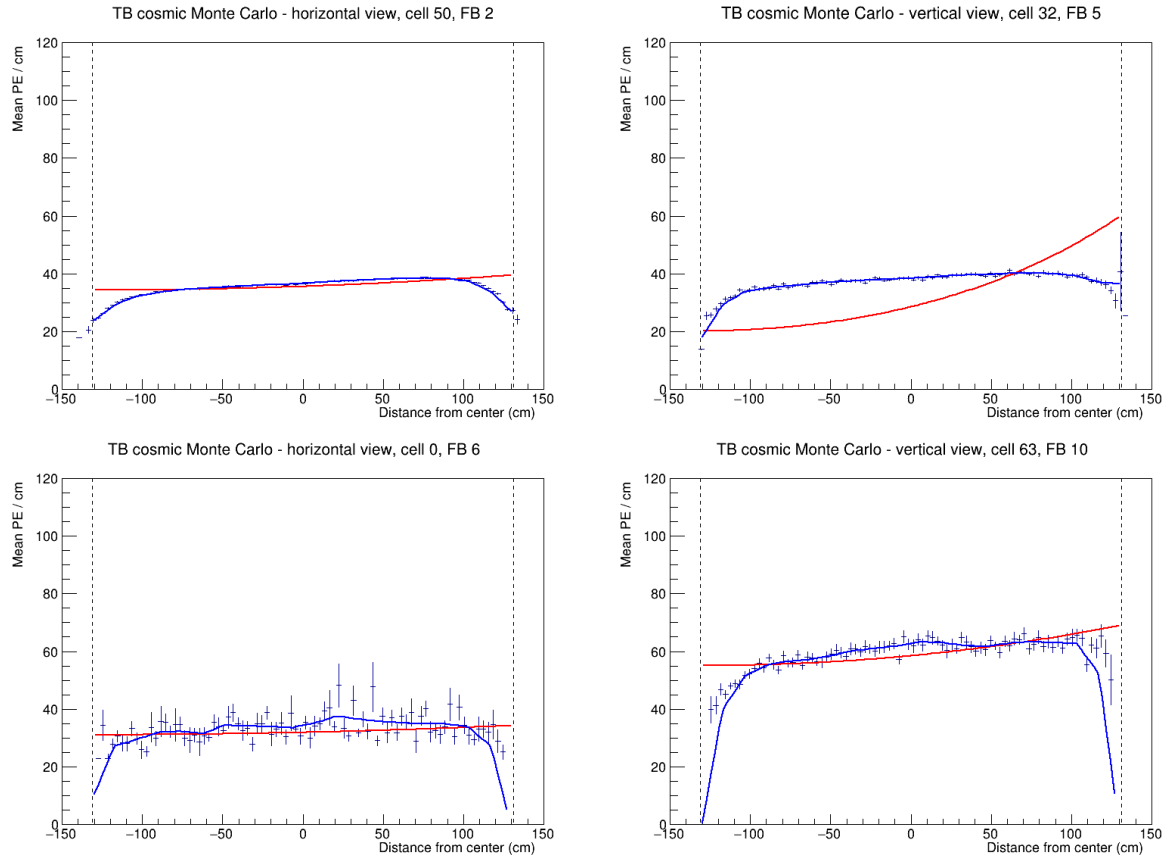


Figure 11: Attenuation fits for a selection of cells in the Test Beam calibration simulation. Top left is an example of a successful attenuation fit, top right is a failed fit due to statistical fluctuation in the last bin and the bottom plots show failed fits for cells on the edges of the detector.

333 4.5 Period 2 data

334 The underfilled cells issue described in section 2 was present throughout period 2 data taking.
 335 This can be clearly seen on figure 12, represented by the empty cells 31 and 63 in the horizontal
 336 planes, which were marked as bad channels and therefore ignored during processing. This also
 337 affects the neighbouring cells to the underfilled cells, which have fewer events due to the tricell
 338 condition.

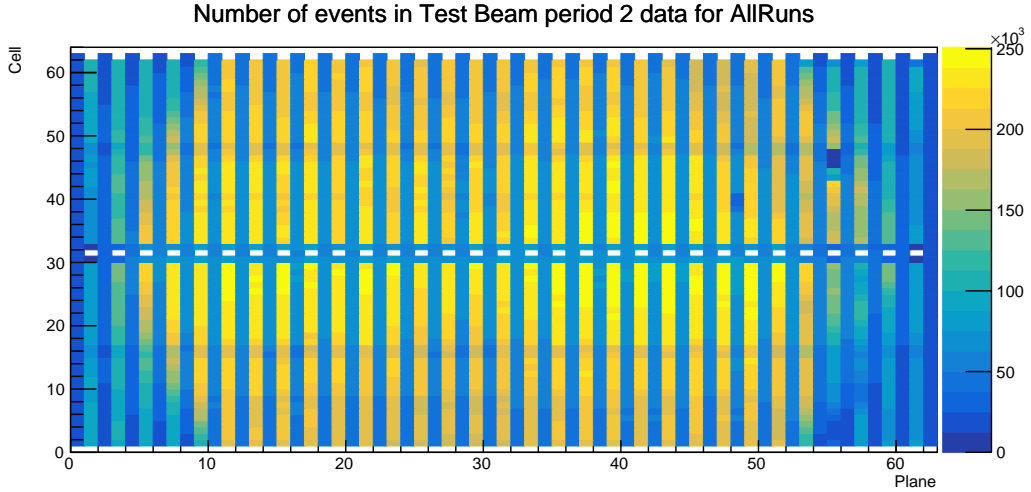


Figure 12: Distribution of events in the period 2 Test Beam data calibration sample.

339 There was also an issue of switched cables from the readout in plane 55 between cells 3 and
 340 46 [?], which can also be seen on figure 12. This is manifested as fewer total number of events
 341 in those cells and in their neighbours, again due to the tricell condition.

342 Officially, period 2 is divided into 6 epochs 2a - 2f, compared on figures 13, 14 and 15. The
 343 epochs mostly differ in the use of various FEB firmwares, with epoch 2c being a trigger study
 344 with paddles. As can be seen on the plots, the individual epochs vary only slightly, only in a
 345 small normalization. We decided to use the entire period 2 without splitting it into any smaller
 346 samples for calibration.

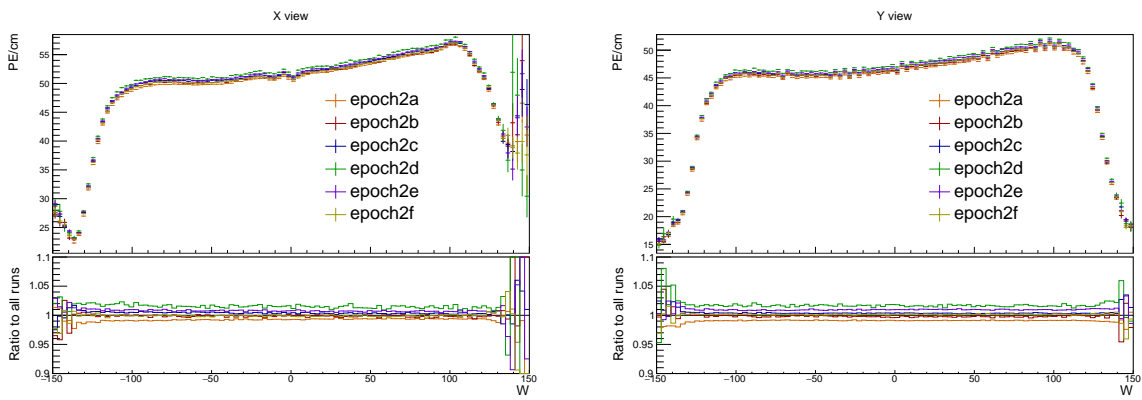


Figure 13: Uncorrected average energy response as a function of the position within a cell (w) for epochs in period 2. It is clear that there is no significant difference between the various epochs.

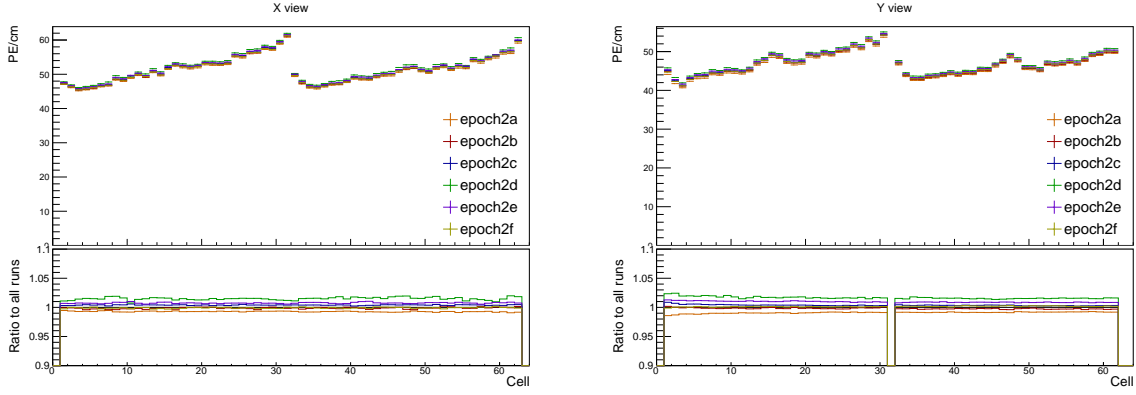


Figure 14: Uncorrected average energy response as a function of cells for epochs in period 2.

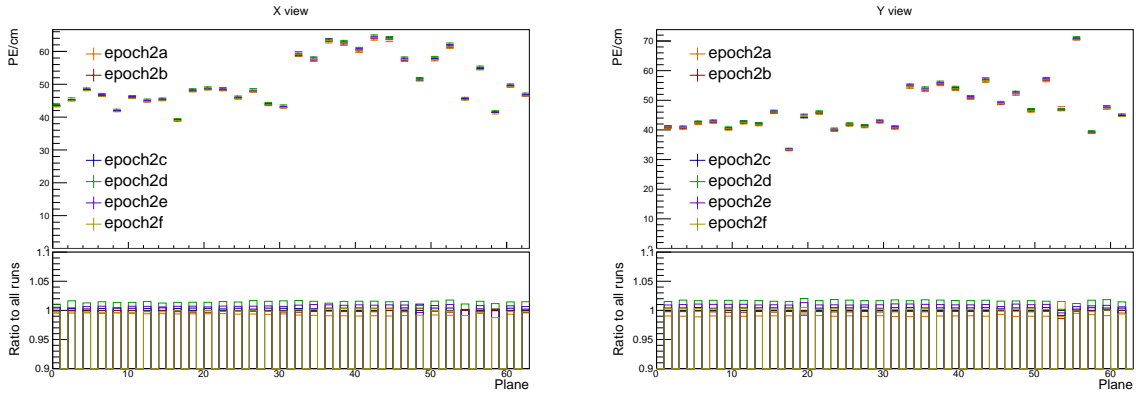


Figure 15: Uncorrected average energy response as a function of planes for epochs in period 2.

347 Period 2 relative calibration results

348 The results of the attenuation fit for period 2 are summarised on figure 16 showing the fitted
349 response at the centre of each cell, or blank cell if the cell failed calibration.

350 Most of the cells have the expected response, as shown on the left plot of figure 17. Here
351 the mean response in PE/cm slowly and approximately constantly rises towards the readout
352 (right side of the plot) and drops down on the cell edges, marked with dashed lines.

353 Some cells have a non-flat response across the cell, with one or more regions with lower
354 energy response, as shown on the right plot of figure 17. These low regions are (almost cer-
355 tainly) a real physical effect caused by zipped, or possibly even twisted fibres [?], present in all
356 of NOvA's detectors. Relative calibration corrects for this effect in data, but zipped fibres are
357 not included in simulation, for any of the detectors. This could potentially cause issues with
358 the ADC threshold in simulation.

359 Since the underfilled cells were marked as bad channels we didn't even attempt to calibrate
360 them. Their neighbours have fewer events due to the tricell condition but majority of them
361 pass the calibration condition, as shown on figure 18. The neighbouring cells in plane 1 don't
362 pass the calibration due to low statistics and therefore large fluctuations, as shown on figure 19.
363 This is likely due to a combination of the tricell condition and plane 1 being on the edge of the
364 detector, which typically has fewer (accepted) hits than the center as shown on figure 12.

365 The left half of plane 55 has $> 3 \times$ larger response than it's surrounding planes, as shown

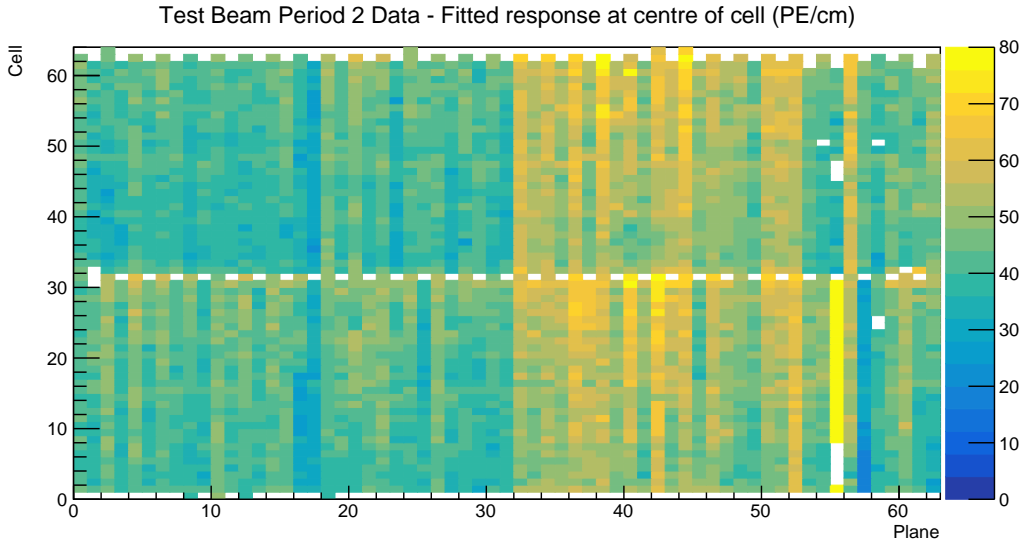


Figure 16: Overview of the relative calibration results for the Test Beam detector period 2 data. Each cell represents the result of the attenuation fit to the energy response in the centre of that cell. The blank cells are uncalibrated.

366 on the left plot of figure 20. Similarly, the left half of plane 57 has lightly lower response than
 367 the surrounding planes, as shown on the right plot of figure 20. This is due to the corresponding
 368 APDs/FEBs faultily recording different energy response than the real energy deposited in the
 369 detector. Since this is present for all data, not only for the cosmic muons used for calibration,
 370 it is important to correctly calibrate them. The issue can arise if these FEBs have been "faulty"
 371 only for a limited time of the entire calibrated period. Since we are doing the attenuation fit on
 372 the profile histograms, if an FEB records a standard response for half of the time and $7\times$ larger
 373 response for the seconds half, calibration is going to assume the response was $4\times$ larger the
 374 entire time, which is incorrect. Since both of these planes are in the back of the detector, we
 375 decided to ignore this effect for period 2.

376 The swapped cables in plane 55 have almost no events, which affects both them and their
 377 neighbours as shown of figure 21.

378 Several cells in the end of the Test Beam detector are uncalibrated due to bins on the edges
 379 of the cell having an unusually high response, or no events at all, as shown on figure 22. It is
 380 unknown if this is a real physical effect, possibly related to the fibres, or unfiltered noise hits,
 381 or something else entirely. Since these cells are in the end of the detector, it is safe to ignore
 382 them.

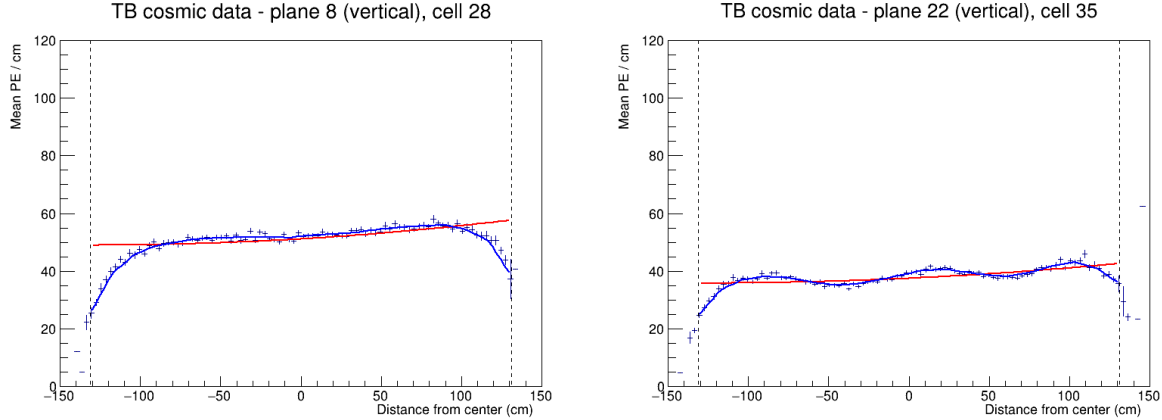


Figure 17: Attenuation fits for a selection of cells in period 2. Left plot shows an example of the standard energy deposition in the Test Beam. Right plot shows the effect of zipped fibres.

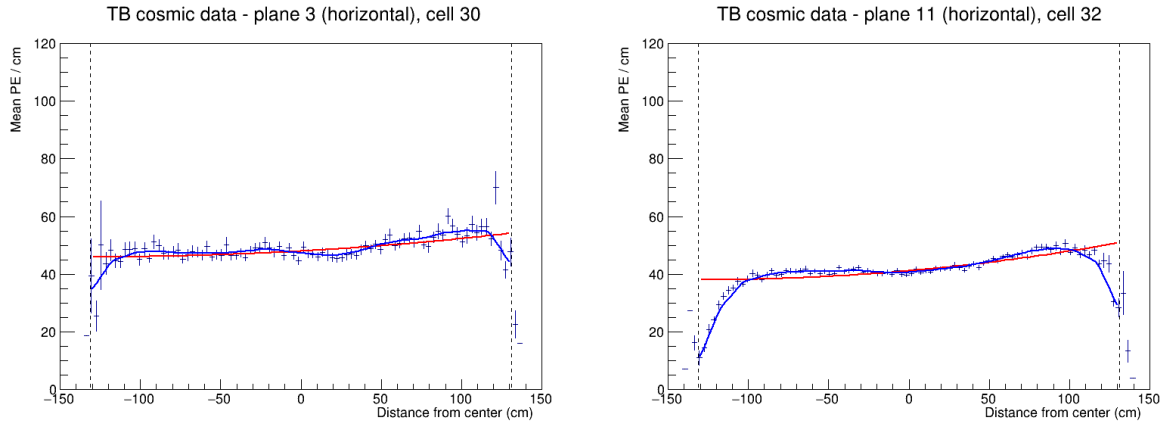


Figure 18: Fit to the energy response in period 2. The cells neighbouring the underfilled cells have fewer events and therefore larger fluctuations than the "usual" Test Beam cell.

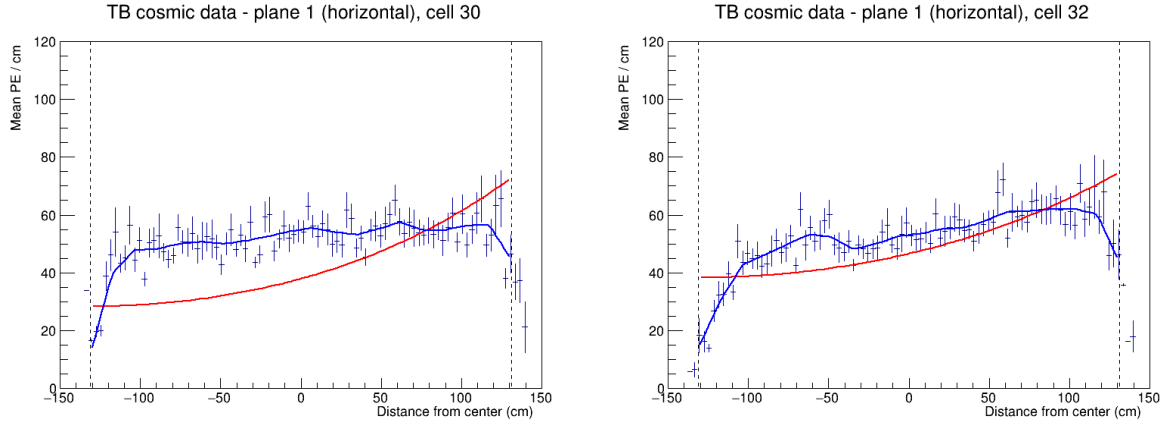


Figure 19: Fit to the energy response in period 2. The neighbouring cells to the underfilled cells in plane 1 are uncalibrated due to low statistics.

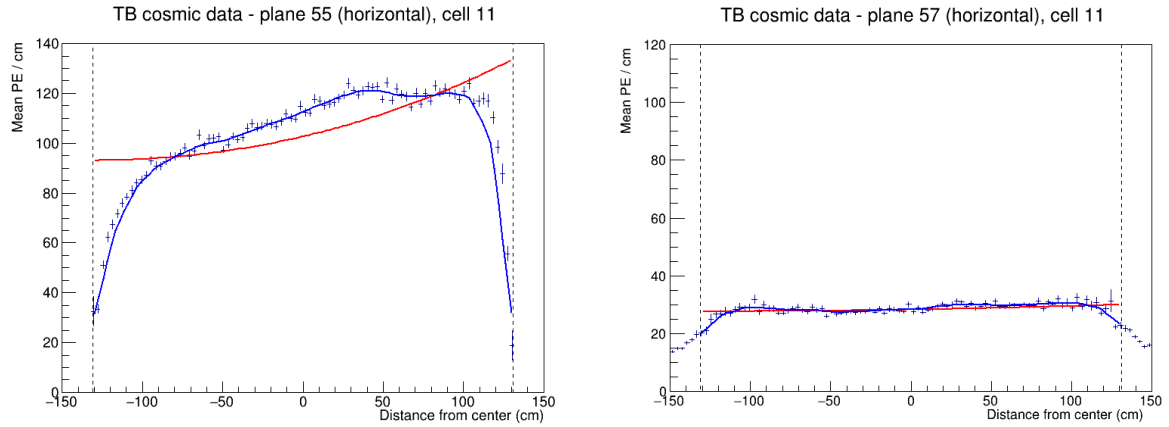


Figure 20: Fit to the energy response in period 2. Lower halves of planes 55 and 57 have a different scale of energy response than the surrounding planes.

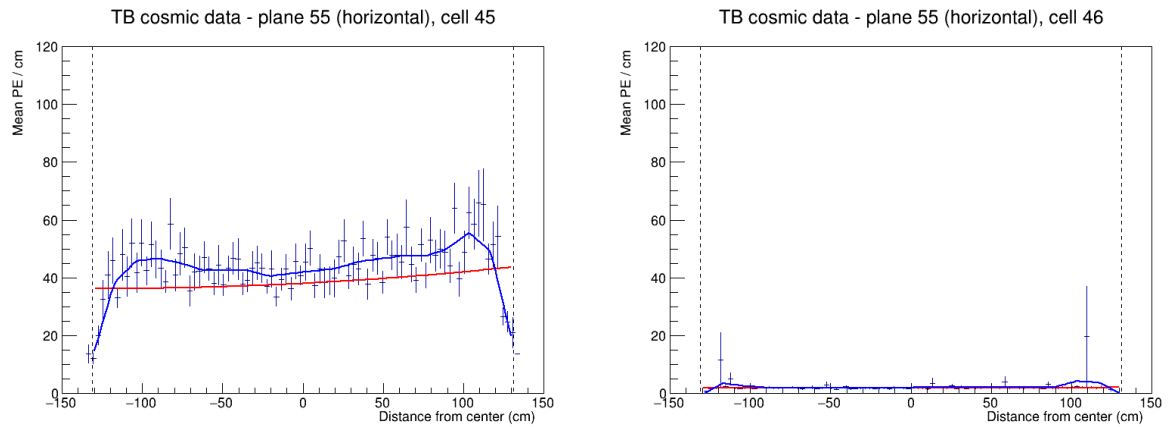


Figure 21: Fit to the energy response in period 2. Cells with swapped readout cables have almost no recorded events as shown on the right plot. This also affect their neighbouring cells due to the tricell condition as shown on the left plot.

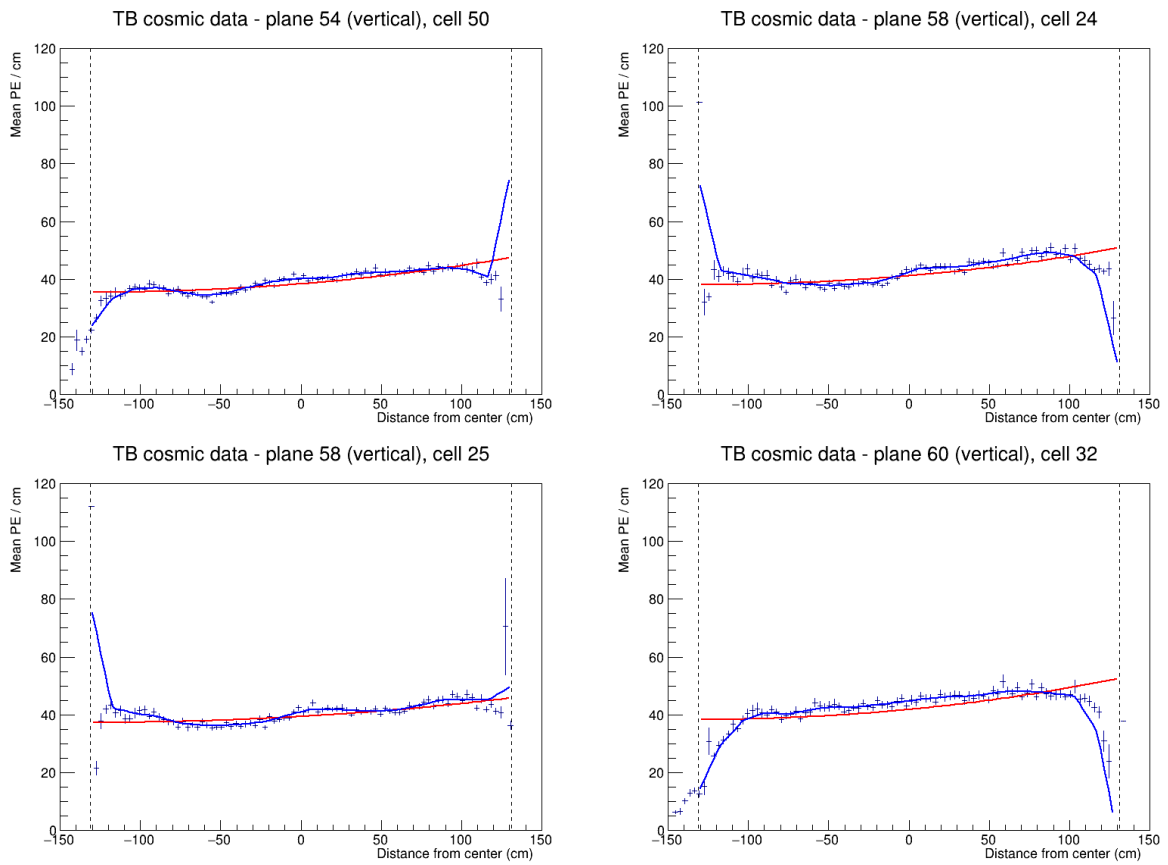


Figure 22: Fit to the energy response in period 2. Examples of cells that have an unusually high or low energy response at the edge of the cell. These cells are not calibrated.

383 4.6 Period 3 data

384 The underfilled cells were refilled (or overfilled) during the period 3 data taking. This was the
385 main motivation for dividing period 3 into individual epochs as shown on table 4. One more
386 major event that could impact the Test Beam data is the replacement of several faulty FEBs,
387 which motivated the creation of epoch 3e.

Epoch 3a	January 12 th 2021	Underfilled cells
Epoch 3b	April 21 st 2021	Overfilling the back 9 horizontal planes and the 7th horizontal plane from the front
Epoch 3c	April 27 th 2021	Overfilling of the 15 front horizontal planes (except the 7th, which was already done) and the 14th horizontal plane
Epoch 3d	April 30 th 2021	Overfilling of the remaining 8 horizontal planes
Epoch 3e	May 12 th 2021	FEB swaps

Table 4: Test Beam period 3 epochs, their start dates and the reason for their separation.

388 The refilling of the underfilled cells can be clearly seen on the cell hits distribution on figure
389 23 and on the distribution of energy deposition across horizontal cells (Y view) on figure 25.

390 From the cell hits distributions we can also see there are a few channels (cells) that were
391 likely dead for a certain time and weren't recording the same number of events as the surround-
392 ing cells. This is specifically plane 48, cell 39 in all of period 3 and plane 18, cell 31 in epochs
393 3d and 3e.

394 The energy distributions across vertical cells and planes (X view) on figures 25 and 26
395 shows, that the top half of plane 58 has a very distinctly different energy deposition compared
396 to the rest of the cells, while having the same number of events, as can be seen on figure 23.
397 This is the most impactful of the faulty FEBs replaced for Epoch 3e.

398 From these discussion, we have decided to calibrate epochs 3a, 3b and 3c together (all
399 epochs containing any underfilled cells) and separately calibrated epochs 3d and 3e. The faulty
400 FEB in plane 58 is far enough in the back of the detector that we didn't find it necessary to
401 calibrate epochs 3d and 3e separately. Also epochs 3b and 3c only contain a few days worth of
402 data, which wouldn't be enough for a successful attenuation fit.

403 Combined epochs 3a, 3b and 3c relative calibration results

404 The results of the attenuation fit are summarised on figure 27 showing cell \times plane distribution
405 of the fitted response at the centre of each cell.

406 We can see that some of the underfilled cells that have been refilled for epochs 3b or 3c are
407 now calibrated thanks to including them into the same attenuation fit. An example of energy
408 deposition in such a cell is on the left plot of figure 28.

409 Same as in period 2 most of the neighbouring cells to the underfilled cells are calibrated,
410 except for cell 32 in plane 1, shown on the right of figure 28, which is also affected by the low
411 statistics at the edges of the detector.

412 There is a couple of notably faulty FEBs with a different energy response than their neigh-
413 bours. Besides the expected top half of plane 58, which has about 5 \times larger response than the

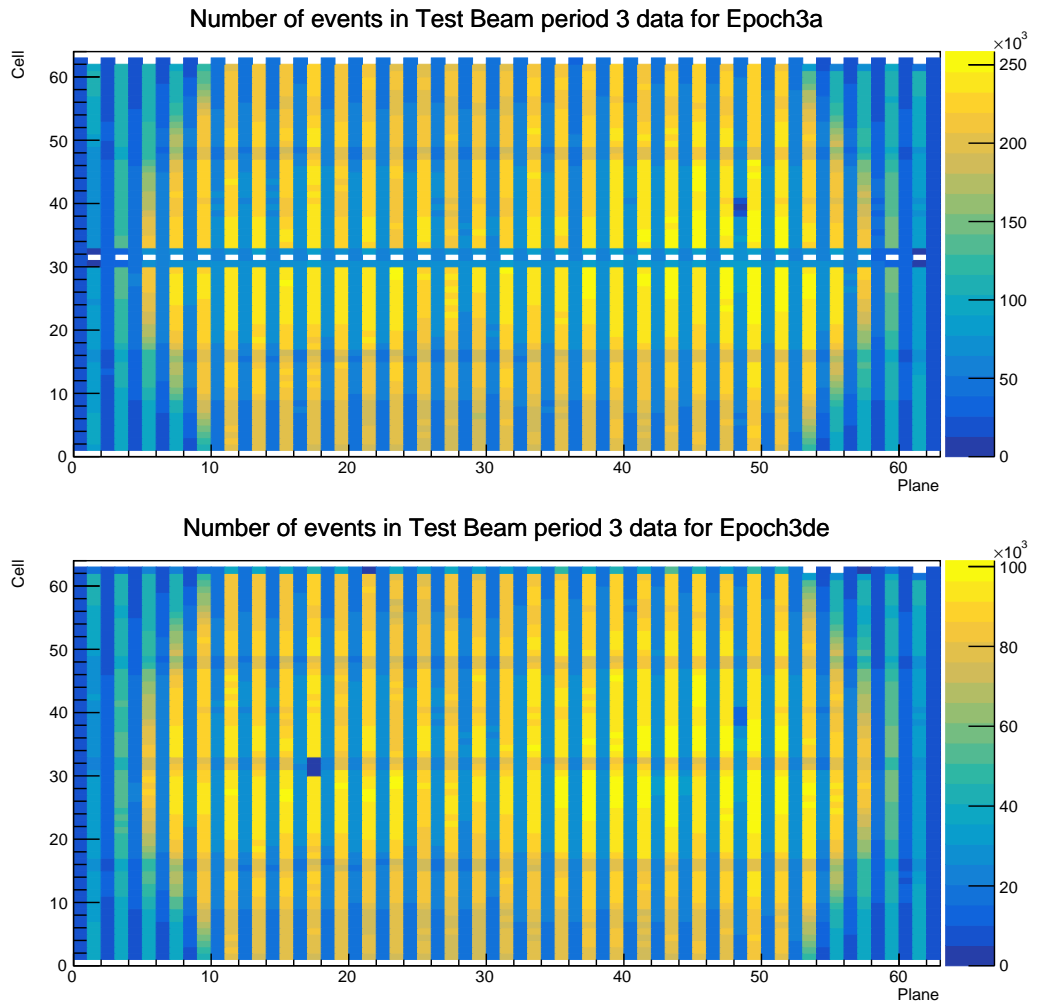


Figure 23: Distribution of events in the period 3 Test Beam data calibration sample. Comparison of Epoch 3a data before the refilling of the underfilled cells and Epoch 3de (combination of Epochs 3d and 3e) after the full refilling.

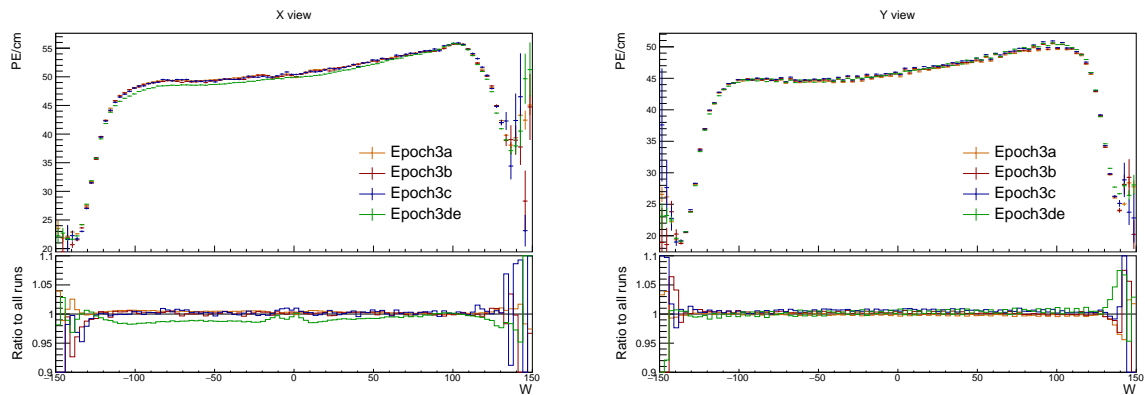


Figure 24: Uncorrected average energy response as a function of the position within a cell (w) for epochs in period 3.

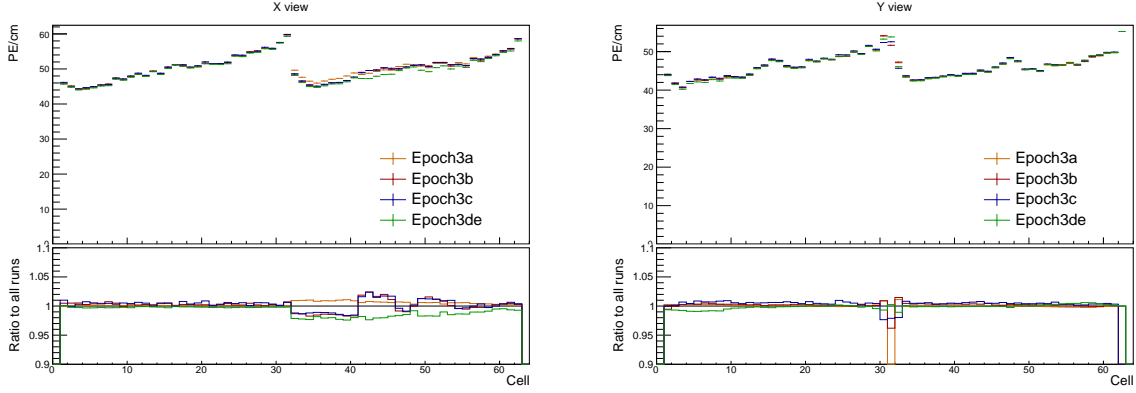


Figure 25: Uncorrected average energy response as a function of cells for epochs in period 3.

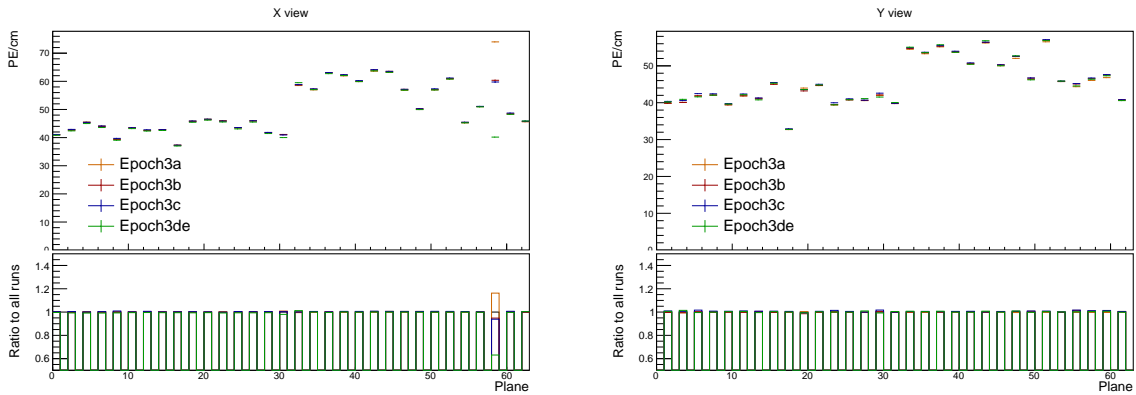


Figure 26: Uncorrected average energy response as a function of planes for epochs in period 3.

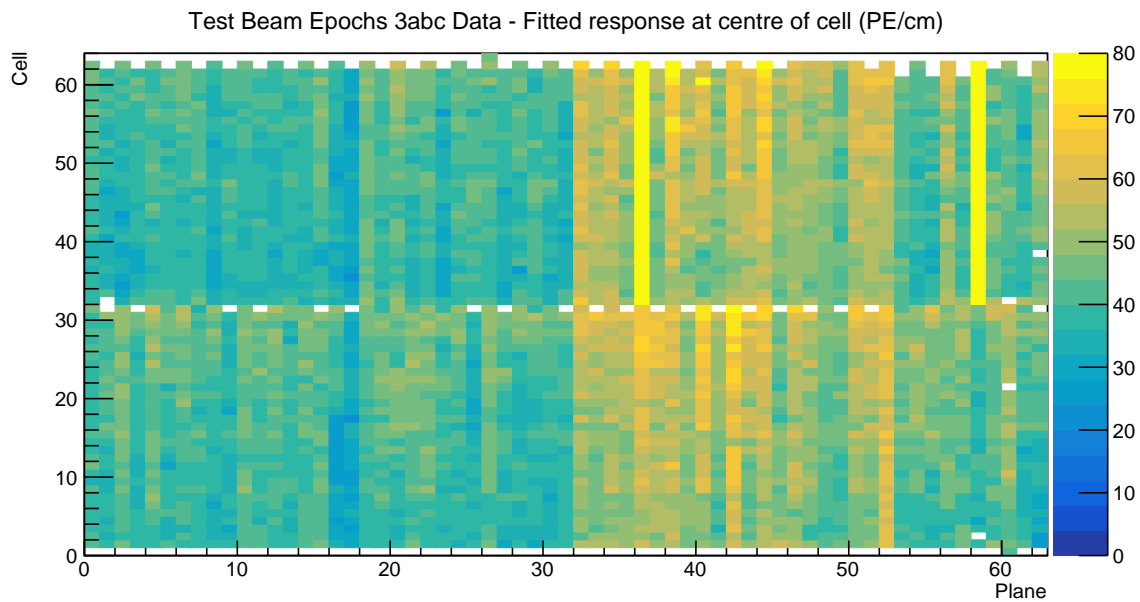


Figure 27: Overview of the relative calibration results for the Test Beam detector period 3, combined epochs 3a, 3b and 3c data. Each cell represents the result of the attenuation fit to the energy response in the centre of that cell. The blank cells are uncalibrated.

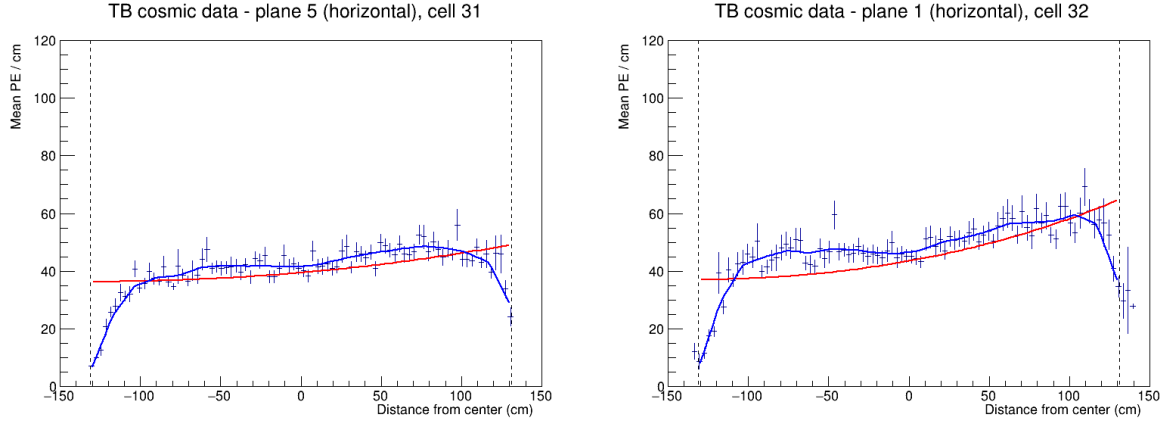


Figure 28: Fit to the energy response in epochs 3 a, b and c. Some underfilled cells that have been refilled in epochs 3b and 3c are now calibrated as shown on the left plot. Cell 32 in plane 1 is the only neighbouring cell to the underfilled cell that didn't manage to get calibrated due to low number of events.

⁴¹⁴ usual, it's also the top half of plane 36, which has about $2.5 \times$ larger response as its neighbours.
⁴¹⁵ This could mean that the FEB in plane 36 was faulty only for a limited time compared to the
⁴¹⁶ FEB in plane 58. The energy deposition for these cells is shown on figure 29.

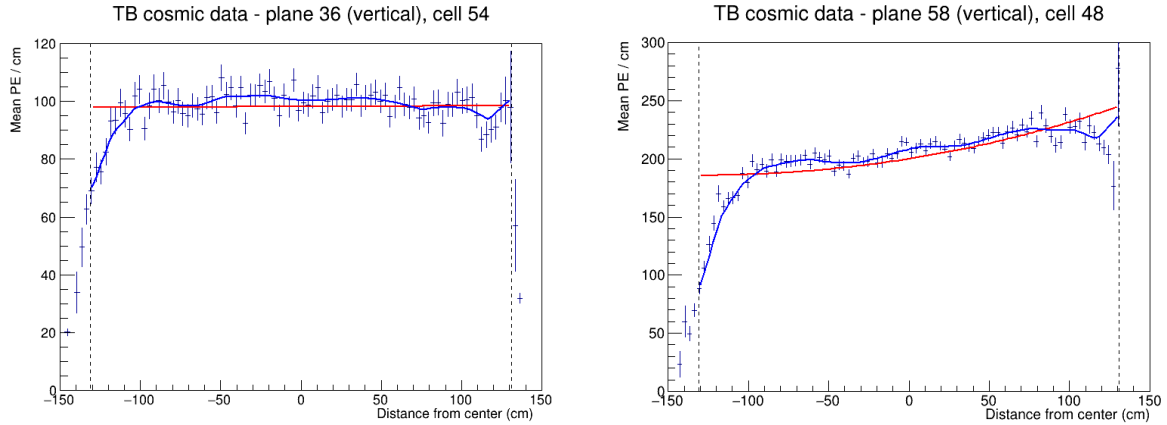


Figure 29: Fit to the energy response in epochs 3 a, b and c. The most obvious faulty FEBs that have a significantly larger energy response than their neighbours.

⁴¹⁷ Similarly as in period 2, there are a few cell in the back of the detector that have a sharp
⁴¹⁸ rise in the energy response at the edge of the cell, which causes them to be uncalibrated. This
⁴¹⁹ can be seen on figure 30.

⁴²⁰ Combined epochs 3d and 3e relative calibration results

⁴²¹ The results of the attenuation fits for epochs 3 d and e are shown on figure 31. There we can
⁴²² see the expected uncalibrated cells in plane 17 related to the dead channel (or possibly still
⁴²³ underfilled cell). The energy deposition for this cell and one of its neighbours is shown on
⁴²⁴ figure 32.

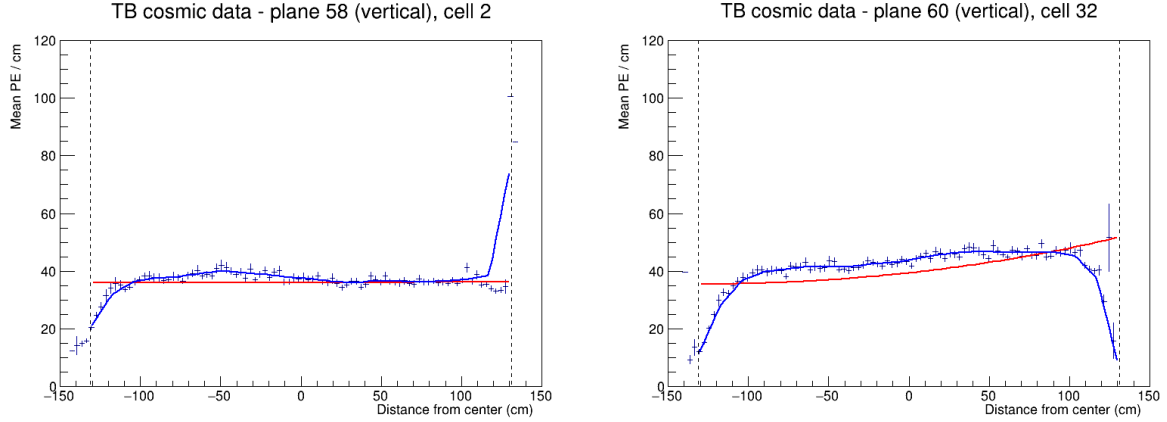


Figure 30: Fit to the energy response in epochs 3 a, b and c. Some cells are not calibrated due to large fluctuations at one edge of the cells.

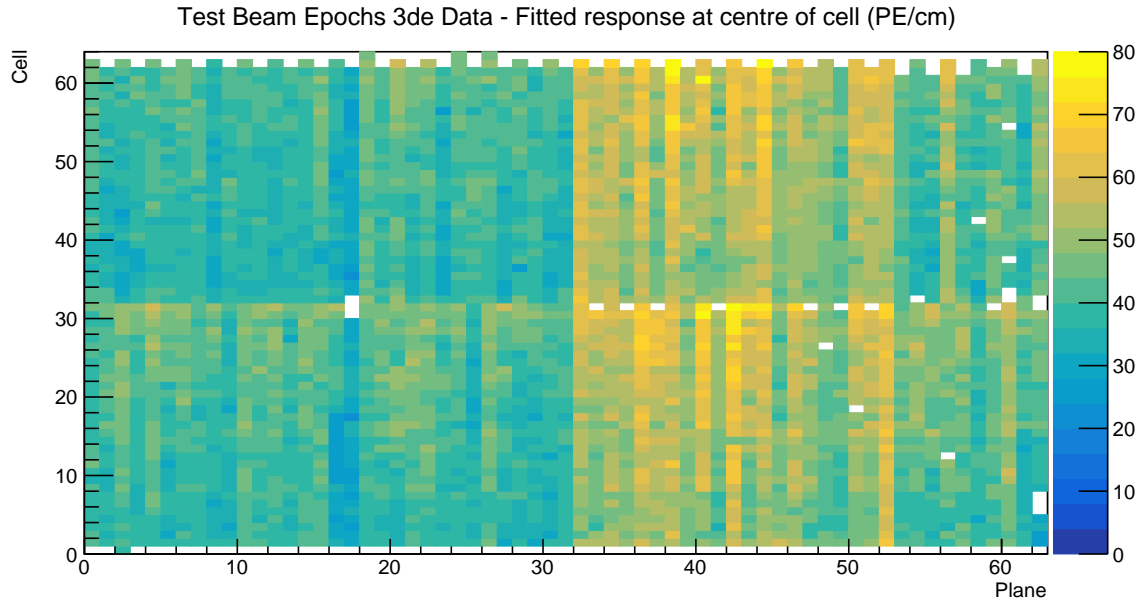


Figure 31: Overview of the relative calibration results for the Test Beam detector period 3, combined epochs 3d and 3e data. Each cell represents the result of the attenuation fit to the energy response in the centre of that cell. The blank cells are uncalibrated.

425 Epochs 3 d and e should have all the previously underfilled cells now refilled, but as can be
 426 seen on figure 31, there's several of these cells that are still uncalibrated. The energy deposition
 427 in these cells is shown on figure 33. We can see that these cells have a fairly large discrepancy
 428 between the left and right side of the cells. This is caused by using different scintillator oils for
 429 the initial filling of the cells and for the refilling. Specifically, these cells have been initially
 430 filled with the Ash River and the Texas oils, which have higher energy depositions compared
 431 to the NDOS oil that was used for the refilling. These oils clearly didn't mix properly which
 432 causes a different energy deposition in different parts of the cells. Since this is a physical effect
 433 that should be accounted for in the calibration and as we can see the fits are actually performing
 434 pretty well and are just confused by the unusual shape. We have therefore decided to manually

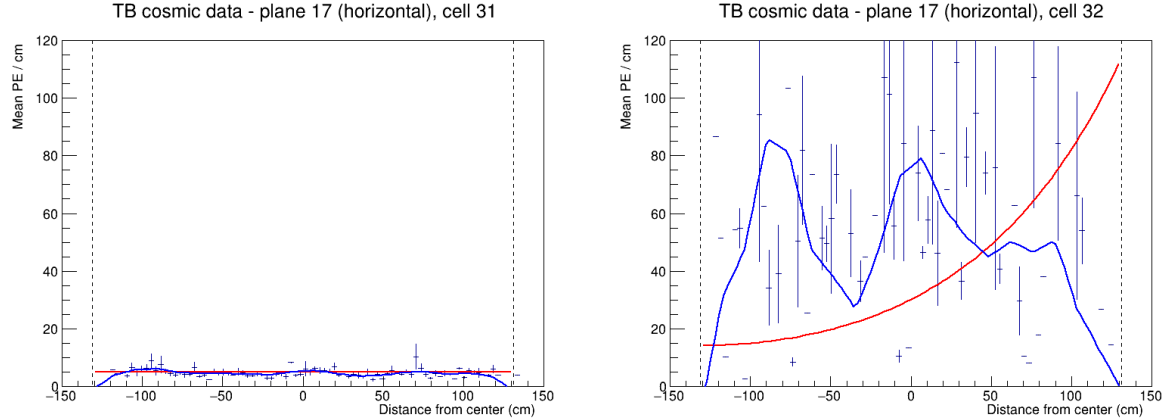


Figure 32: Fit to the energy response in epochs 3 d and e. Possibly dead channel or still underfilled cell.

435 change the χ^2 inside the cvs tables (results of the attenuation fits), so that the $\chi^2 < 0.2$ and
436 these cells are considered calibrated.

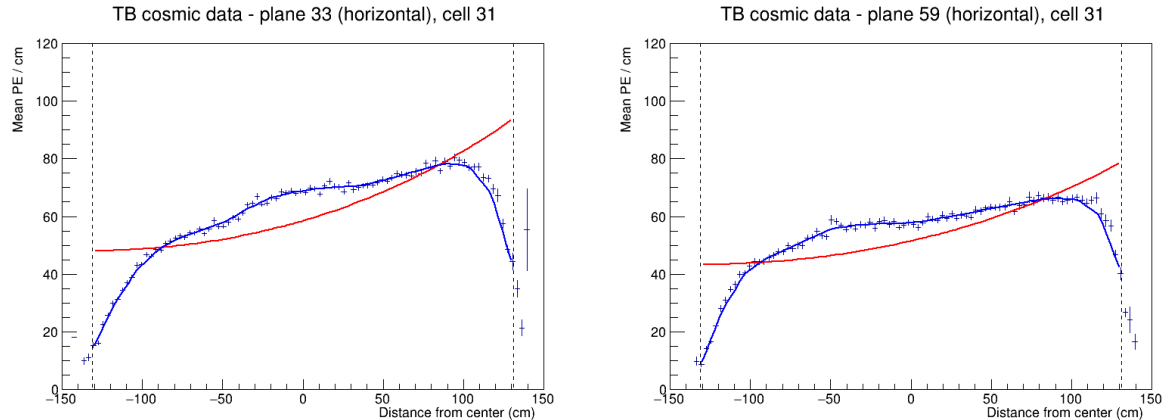


Figure 33: Fit to the energy response in epochs 3 d and e. The scintillator oil used for refilling of the underfilled cells has lower energy response than the oil used for the initial filling. These oils didn't mix properly causing a different energy response in the left and right side of the cell.

437 Some of the cells in the back of the detector have a rise, or drop in energy deposition at the
438 edge of the cell, as can be seen on figure 34. This is similar to the effect seen in period 2 and
439 epochs 3abc and since it's again concentrated in the end of the detector we ignored these cells
440 and left them uncalibrated.

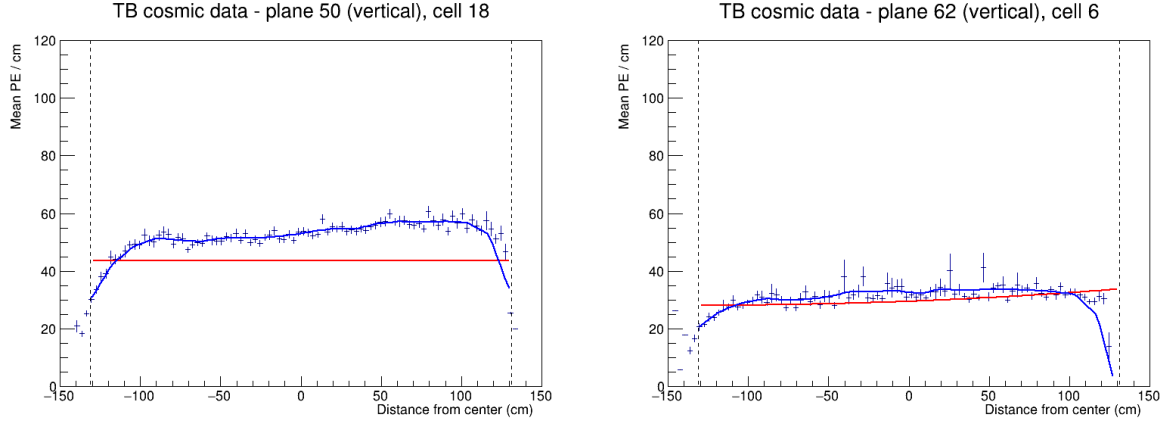


Figure 34: Fit to the energy response in epochs 3 d and e. Some cells have a drop, or a rise of energy response at the edge of the cell. This can be caused by low statistics.

441 4.7 Period 4 data

442 The period 4 Test Beam data taking period is the best data we managed to collect with almost an
 443 ideal condition of the detector. There's only a few commissioning runs in the very beginning,
 444 which uncovered some dead channels or faulty FEBs that have been fixed. These runs make
 445 epoch 4a shown on the top plot of figure 35.

446 There has also been a cell masking study [reference], during which we masked parts of the
 447 front of the detector to help with FEB saturation. We can clearly see this on the middle plot of
 448 figure 35.

449 Figures 36, 37 and 38 show that the epoch 4a and the cell masking study did have a notice-
 450 able impact on the energy deposition across the detector. We have therefore decided to ignore
 451 these runs and only use the rest of the period 4 data for the calibration.

452 Period 4 relative calibration results

453 Results of the attenuation fits for period 4 are summarised on figure 39.

454 We can see that majority of the detector is calibrated, besides some cells on the edge of the
 455 detector, a few formerly underfilled cells (left plot on figure 40) and one cell with an unusually
 456 high response at the edge of the cell (right plot on figure 40). We treated the formerly underfilled
 457 cells the same way as in epochs 3 d and e, by manually changing their χ^2 to be < 0.2 and
 458 therefore making them calibrated.

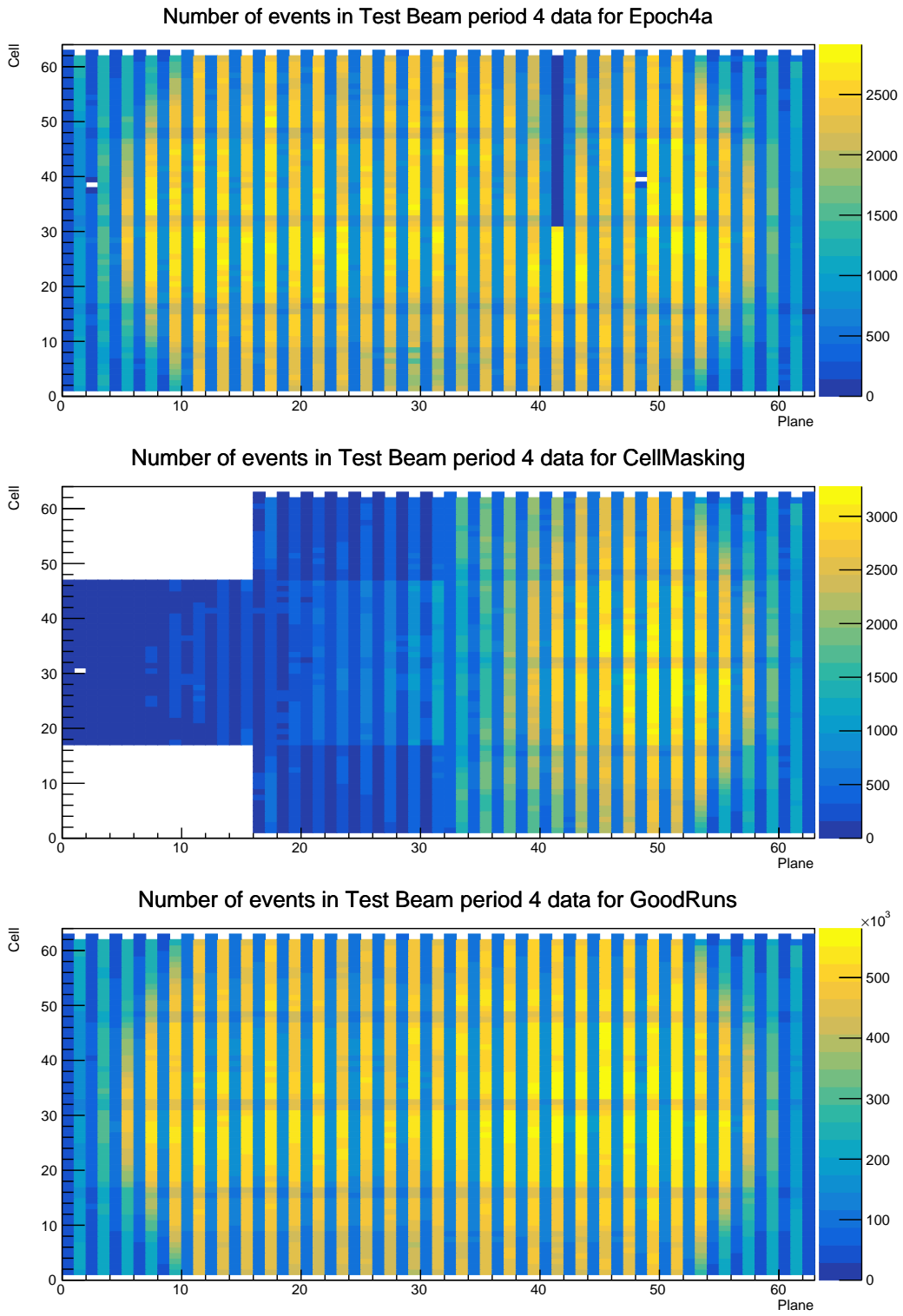


Figure 35: Distribution of events in the Test Beam period 4 data calibration sample. The top plot shows the first three commissioning runs, the middle plot the status of the detector during the Cell Masking studies and the bottom plot shows the rest.

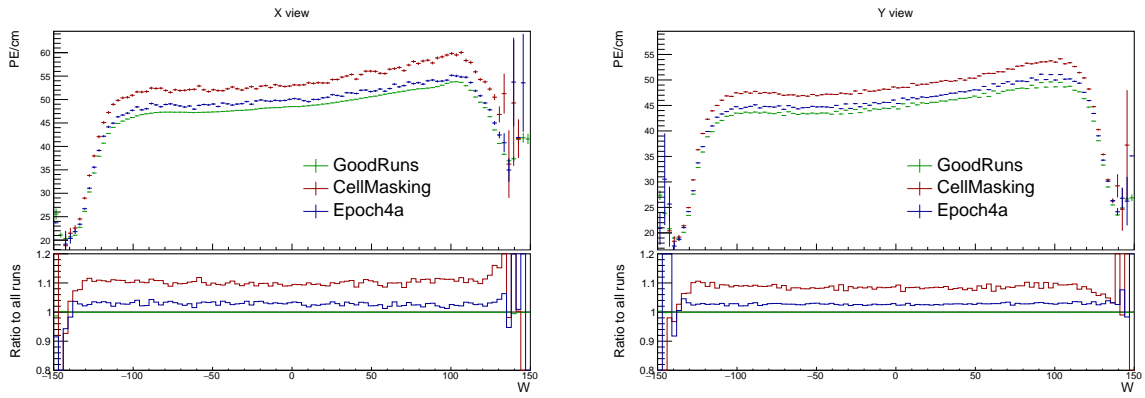


Figure 36: Uncorrected average energy response as a function of the position within a cell (w) for epochs in period 4.

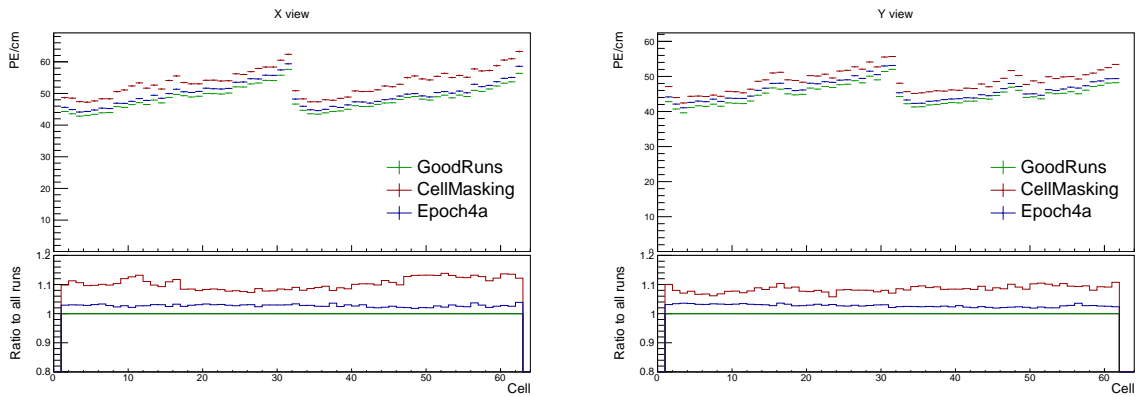


Figure 37: Uncorrected average energy response as a function of cells for epochs in period 4.

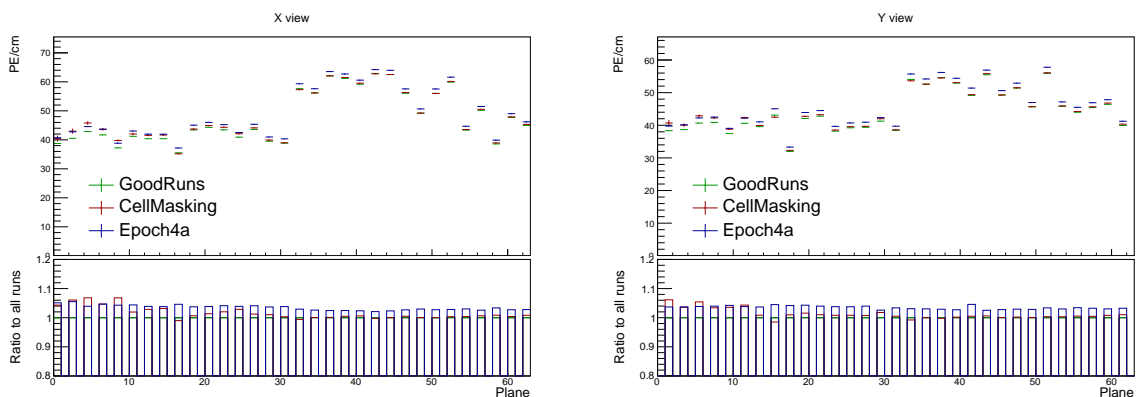


Figure 38: Uncorrected average energy response as a function of planes for epochs in period 4.

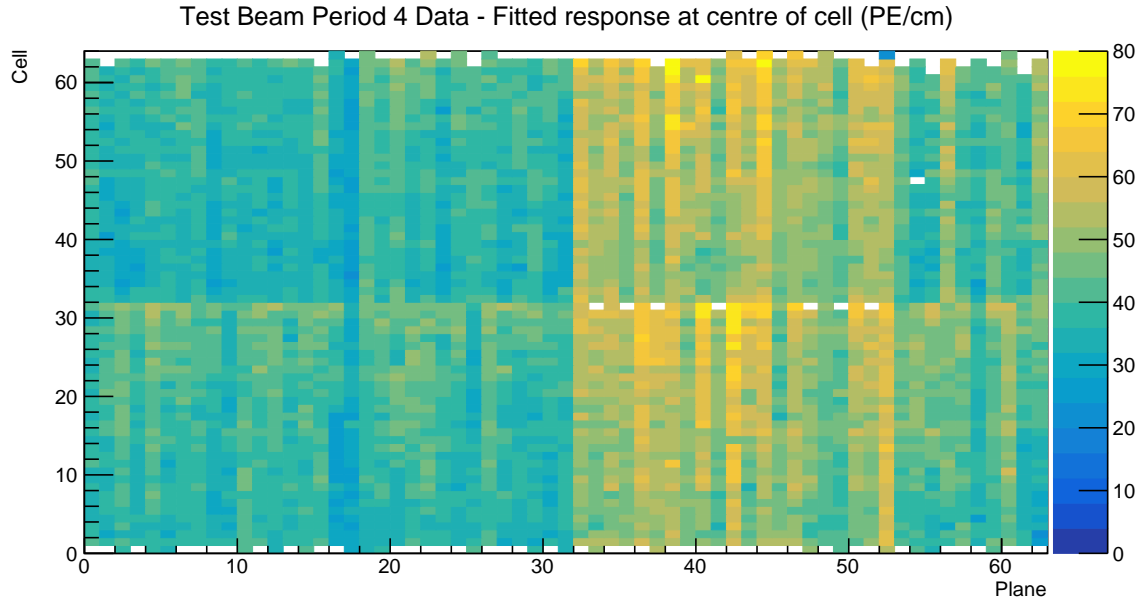


Figure 39: Overview of the relative calibration results for the Test Beam detector period 4 data. Each cell represents the result of the attenuation fit to the energy response in the centre of that cell. The blank cells are uncalibrated.

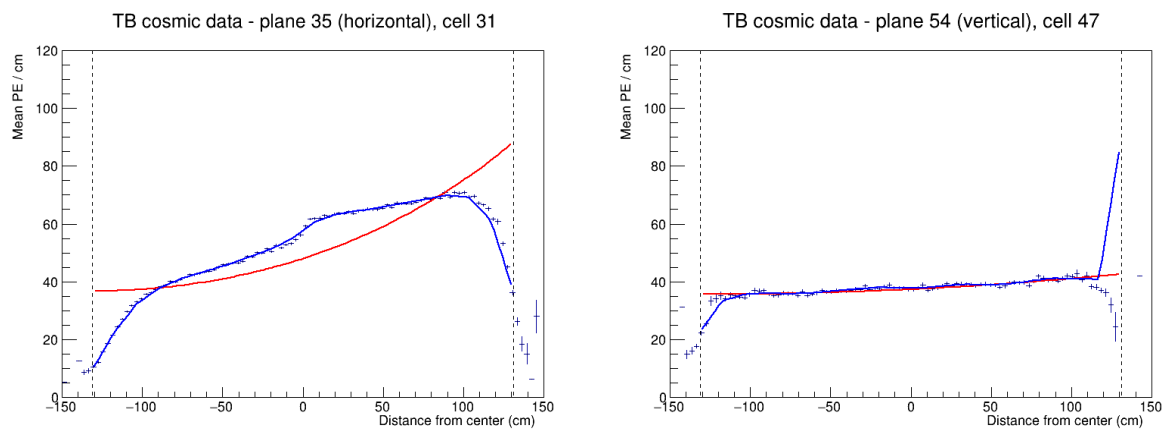


Figure 40: Fit to the energy response in period 4. Previously underfilled cells refilled with a scintillator of a different quality causing an unusual distribution of energy deposition (left). Unusually high energy response at the edge of the cell 47 (right).

⁴⁵⁹ **4.8 Absolute calibration results**

⁴⁶⁰ TO DO: add description of the absolute calibration results, correct the table to fit the page

Sample	NHitsx	MEUx	NHitsy	MEUy	MEU	MEU Err	TrueE/dx	tE/dx Err
epoch 3abc data	2.638e+05	38.49	1.621e+06	39.4	38.94	0.006758	1.772	0.000238
epoch 3de data	1.049e+05	38.63	6.725e+05	39.42	39.02	0.01048	1.772	0.000238
period 2 data	2.322e+05	38.7	1.413e+06	39.4	39.05	0.007252	1.772	0.000238
period 4 data	5.268e+05	38.63	3.316e+06	39.4	39.01	0.004703	1.772	0.000238
simulation	2.829e+05	40.17	1.842e+06	39.93	40.05	0.006418	1.772	0.000238

⁴⁶¹

⁴⁶² **4.9 Results**

⁴⁶³ TO DO: talk about where are the results and what is the final calibration tag

⁴⁶⁴ **4.10 Validation**

⁴⁶⁵ TO DO: describe the validation plots and possibly add more plots

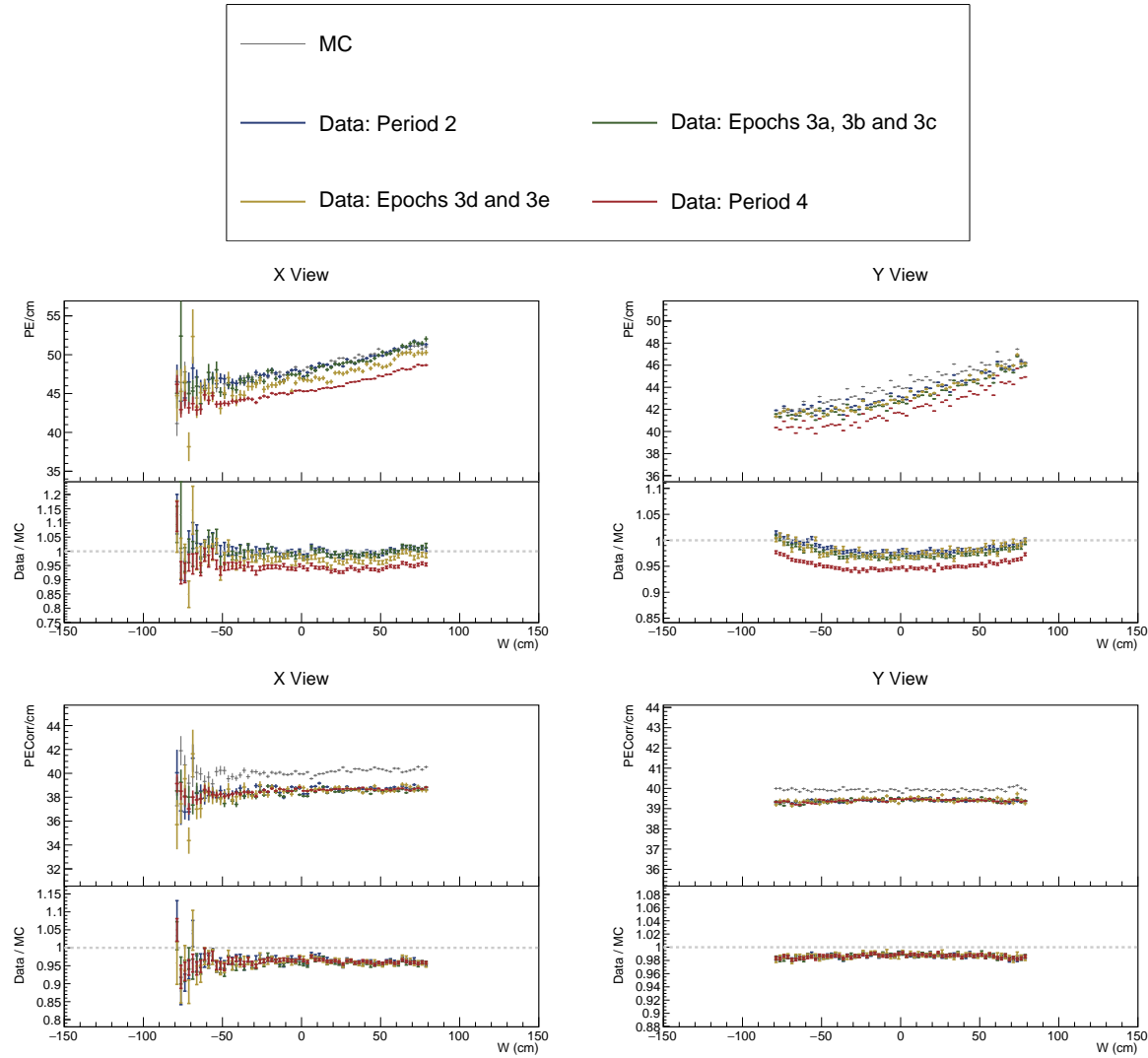


Figure 41: ...

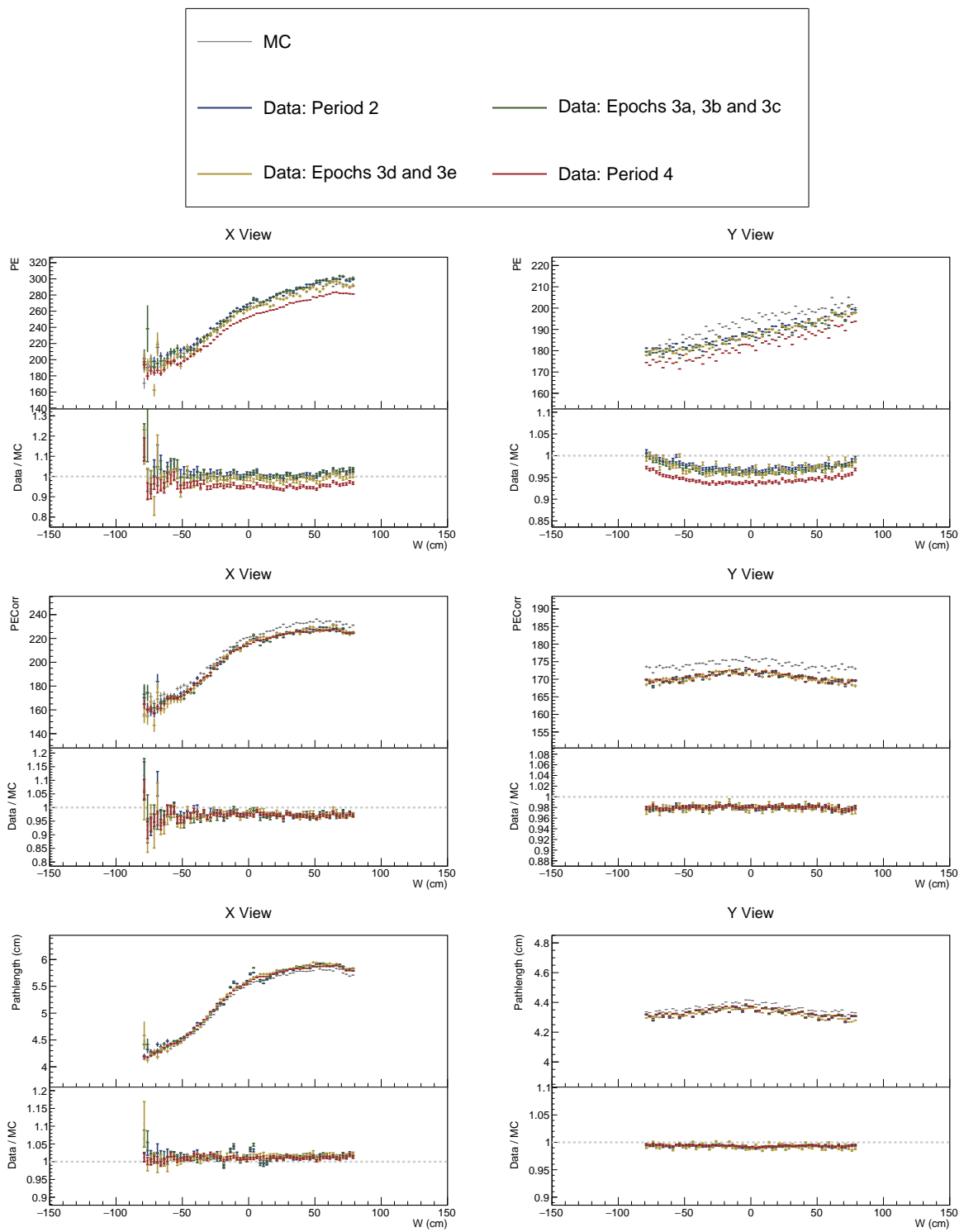


Figure 42: ...

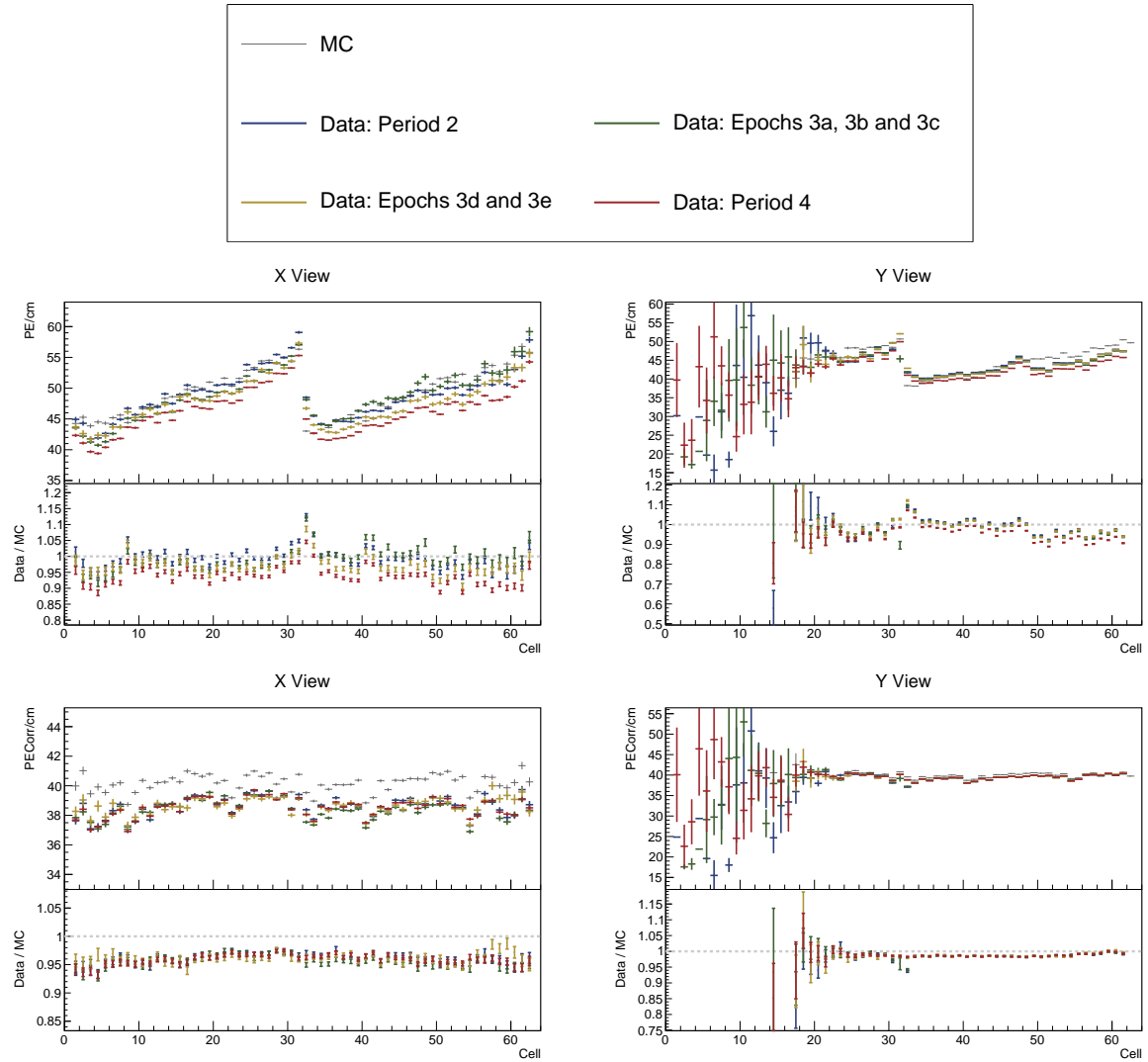


Figure 43: ...

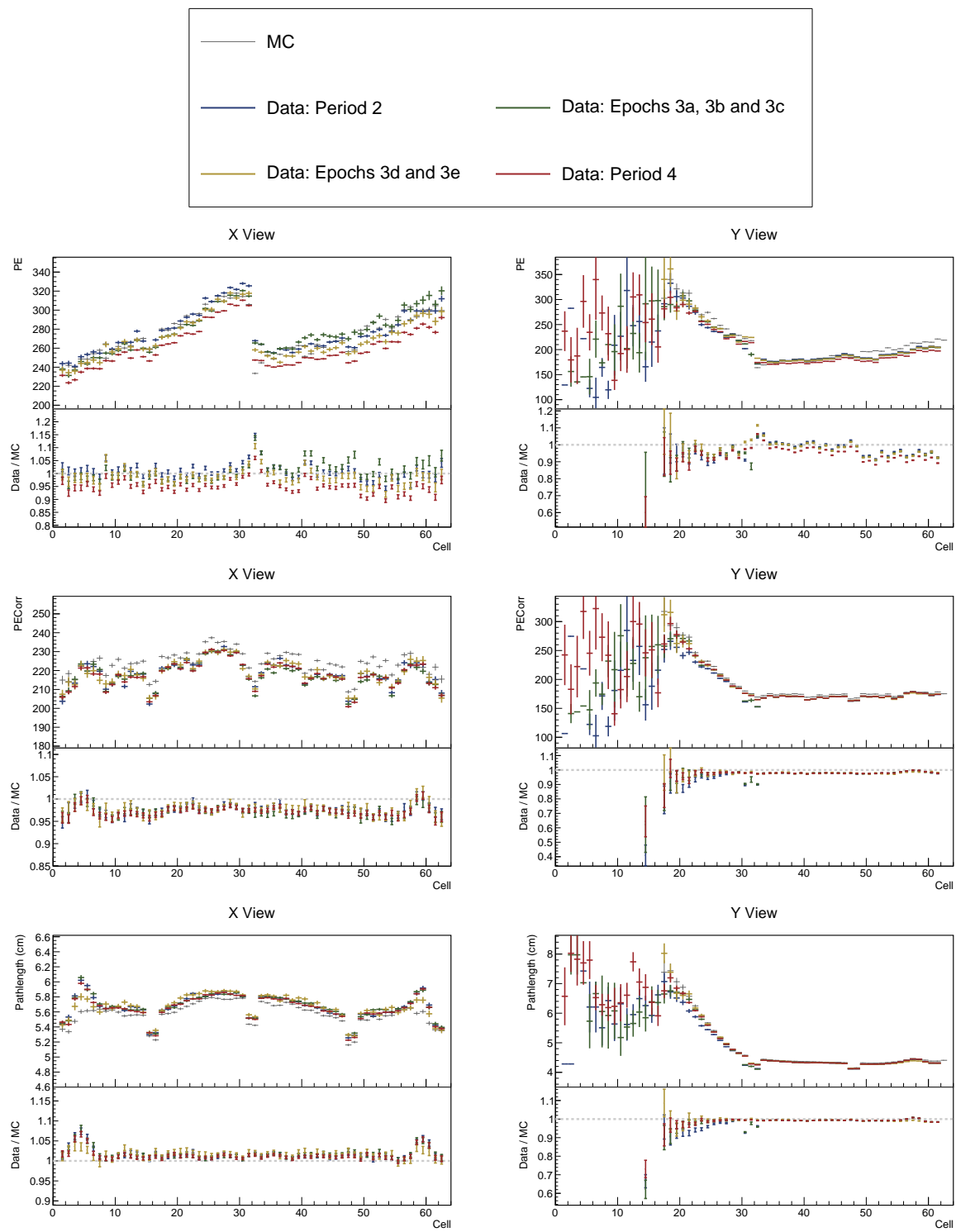


Figure 44: ...

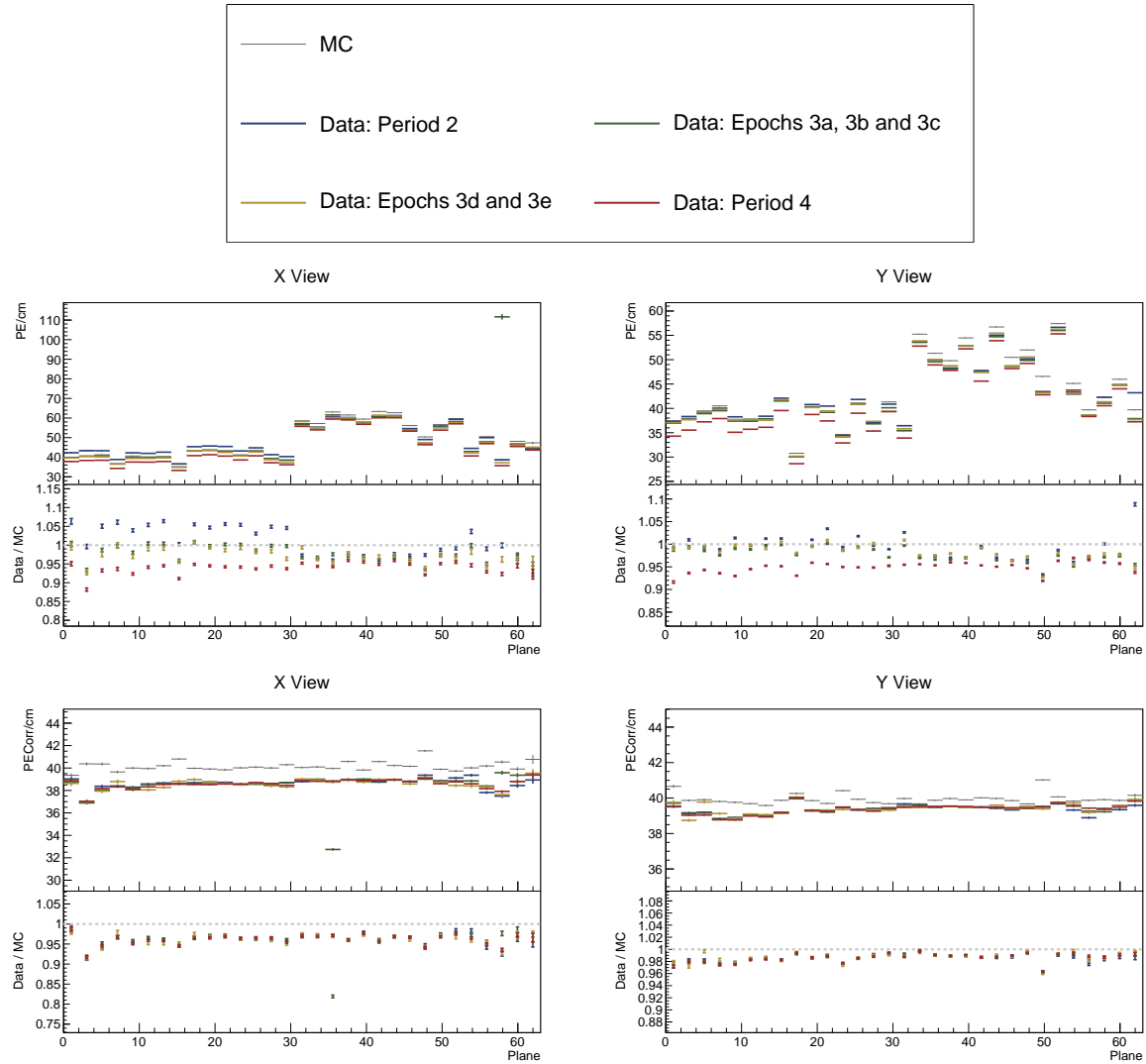


Figure 45: ...

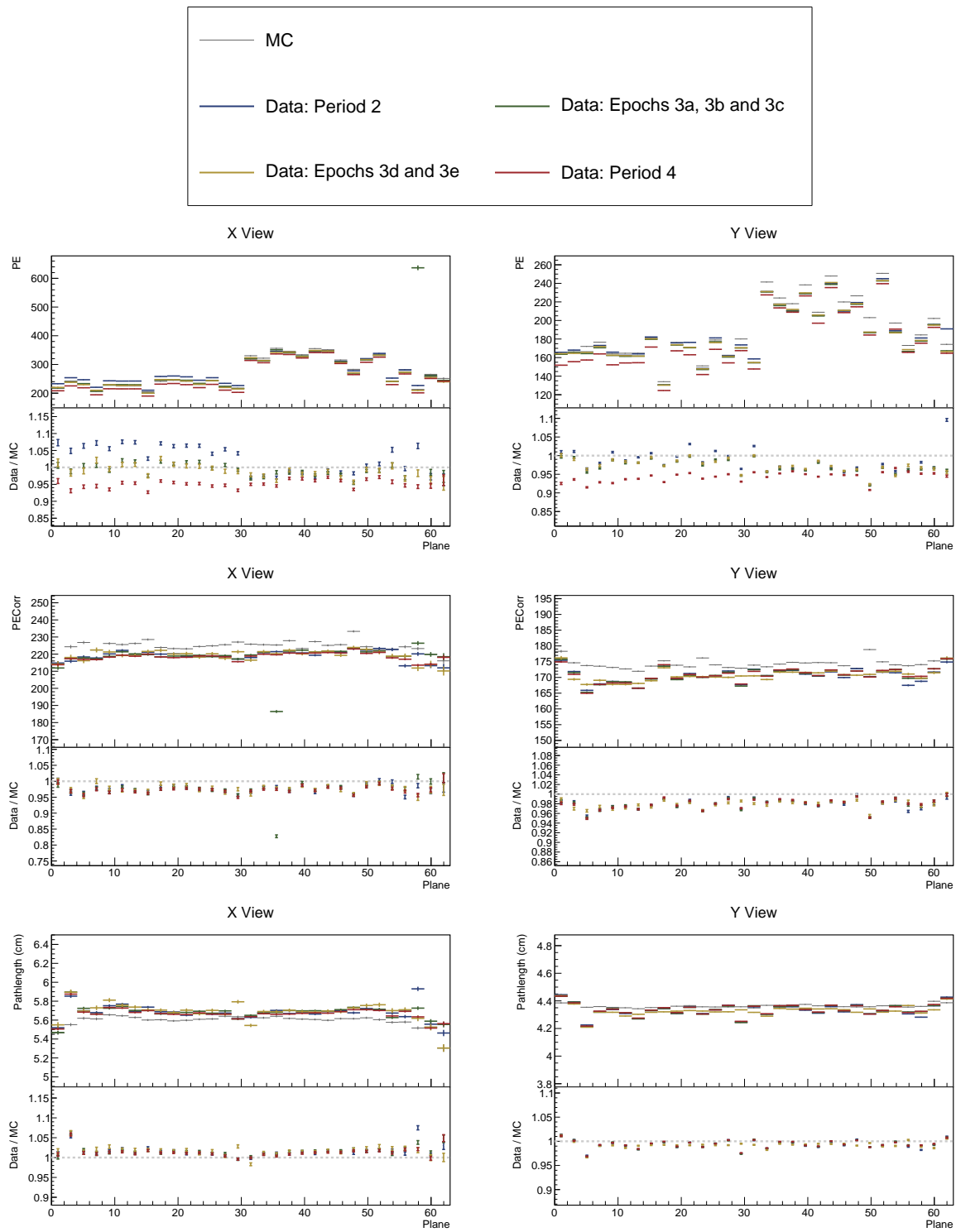


Figure 46: ...

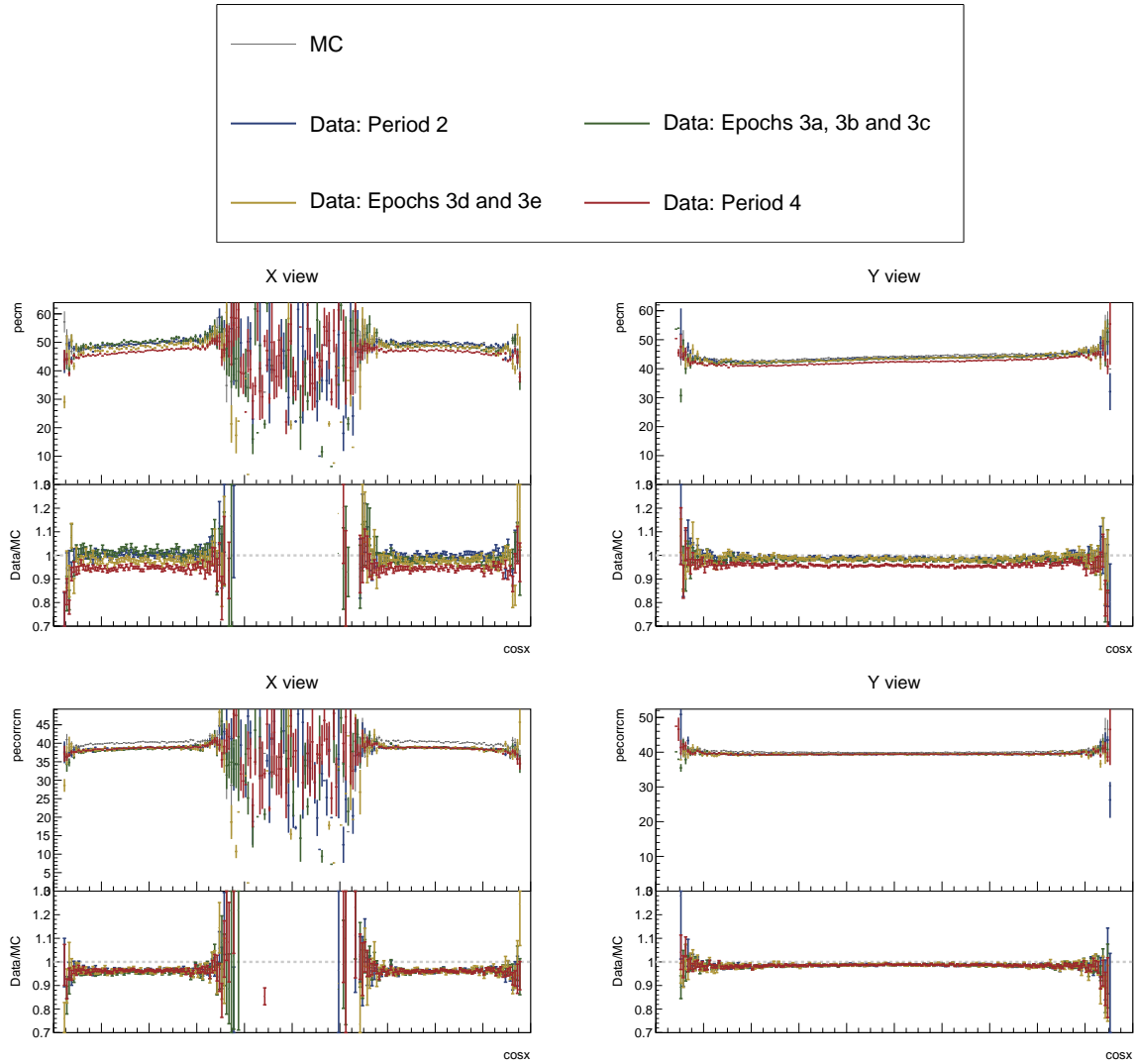


Figure 47: ...

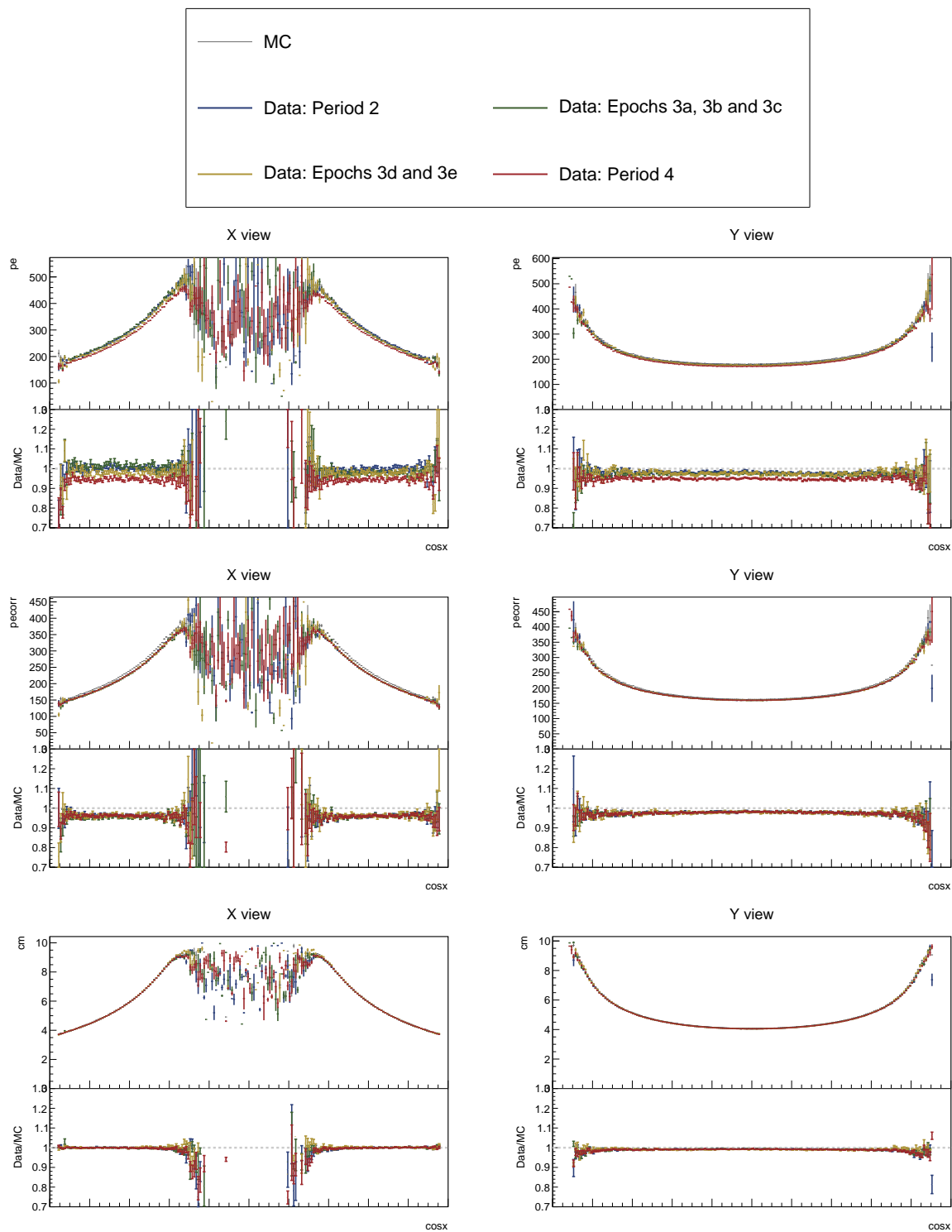


Figure 48: ...

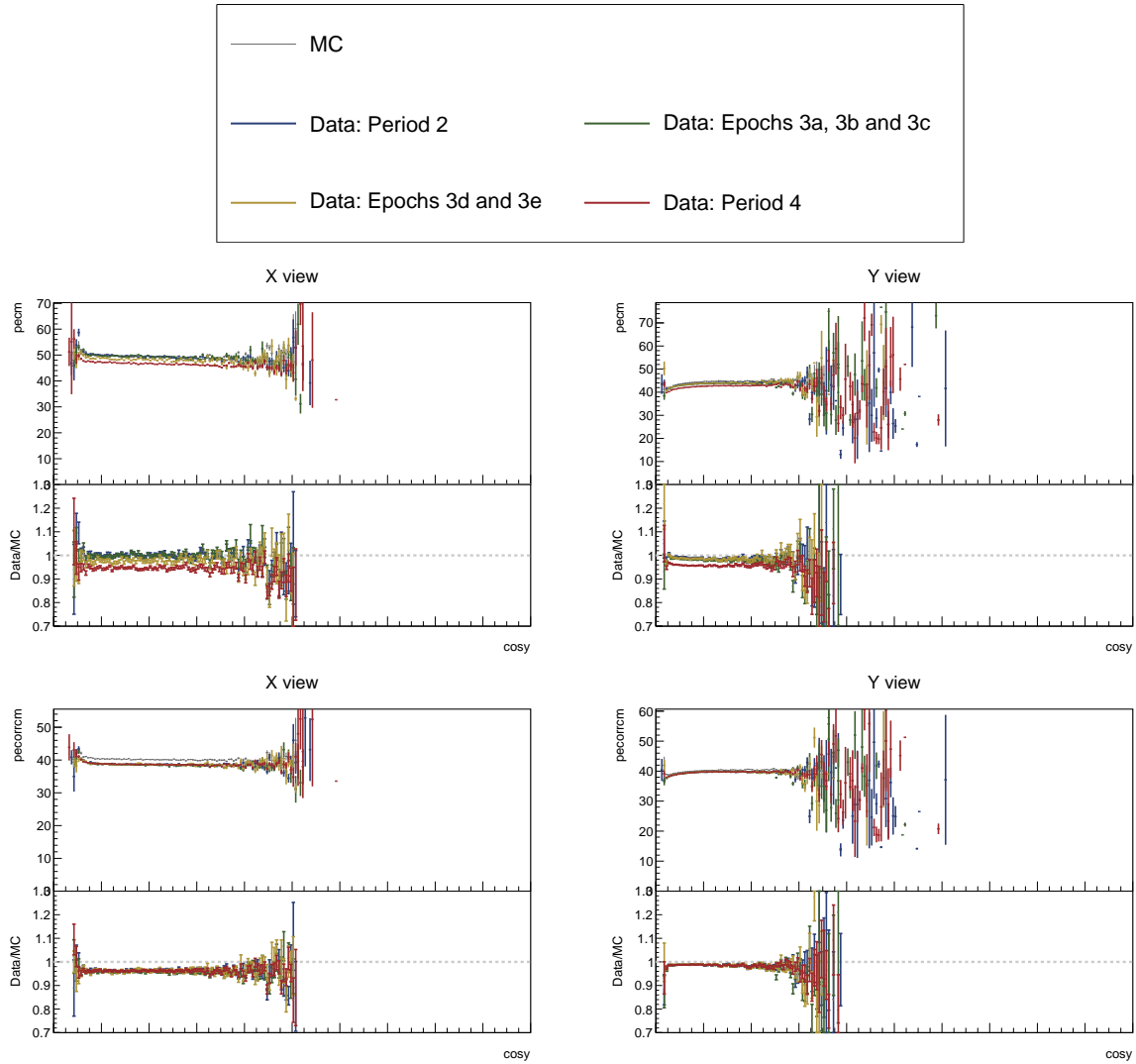


Figure 49: ...

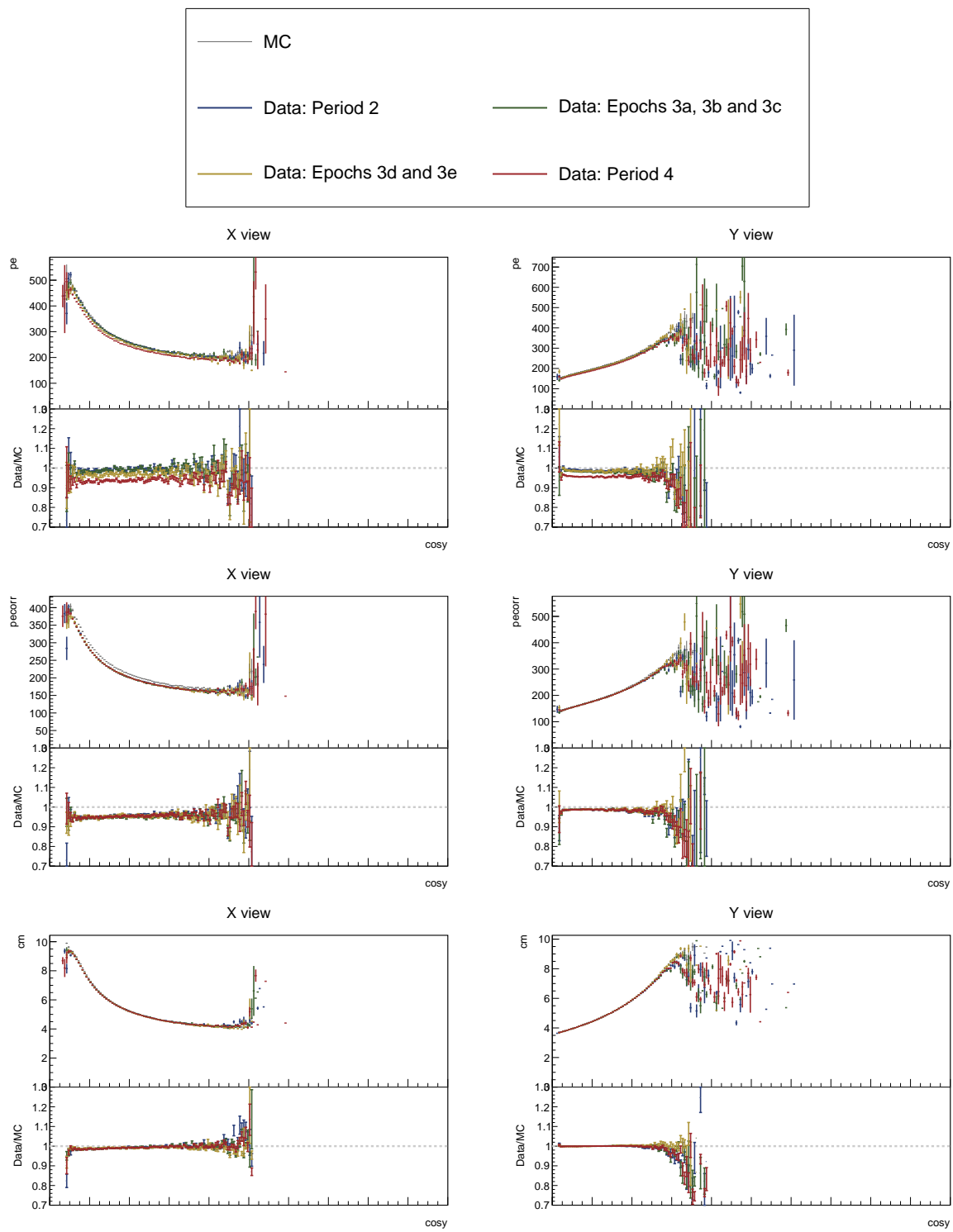


Figure 50: ...

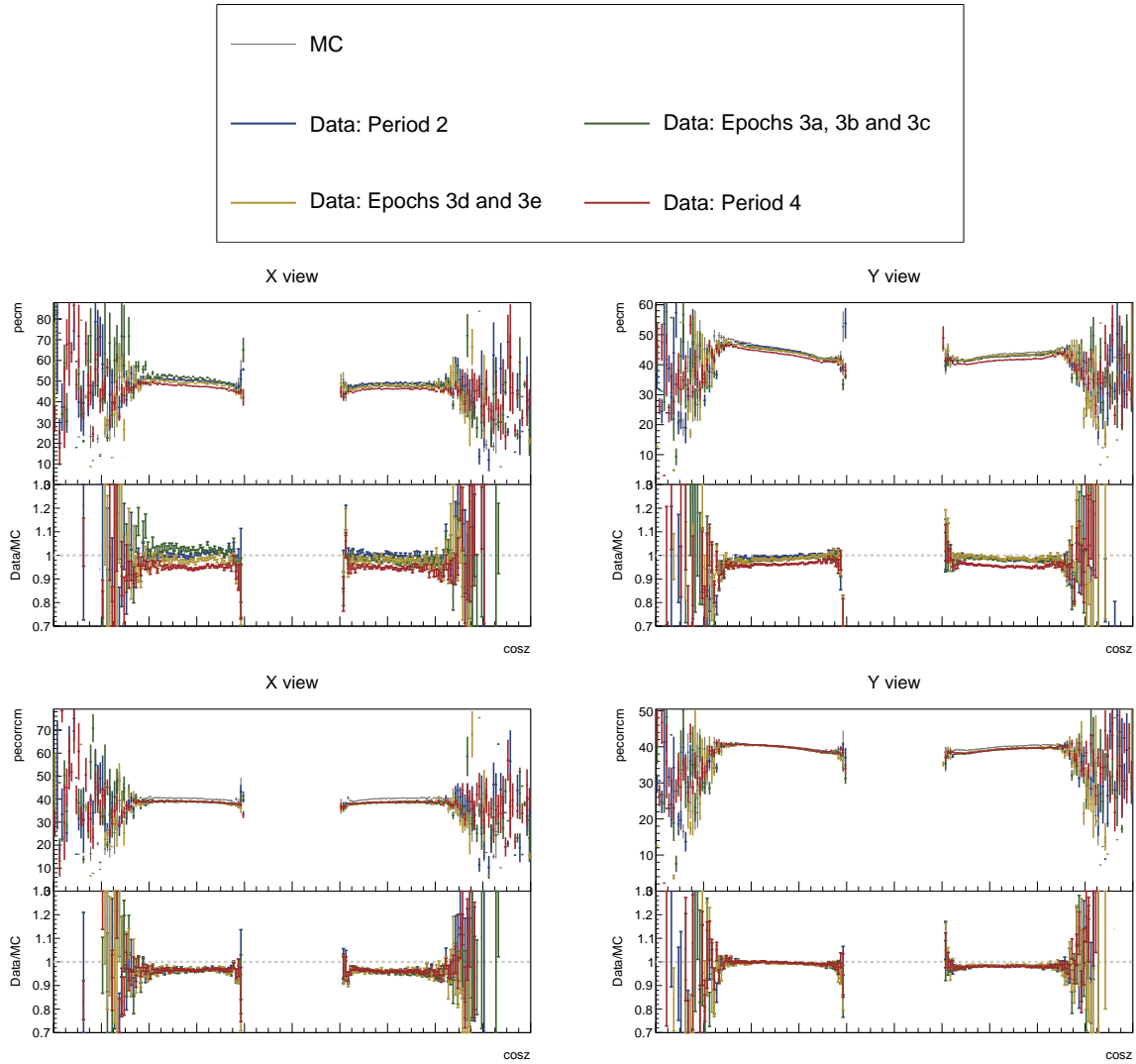


Figure 51: ...

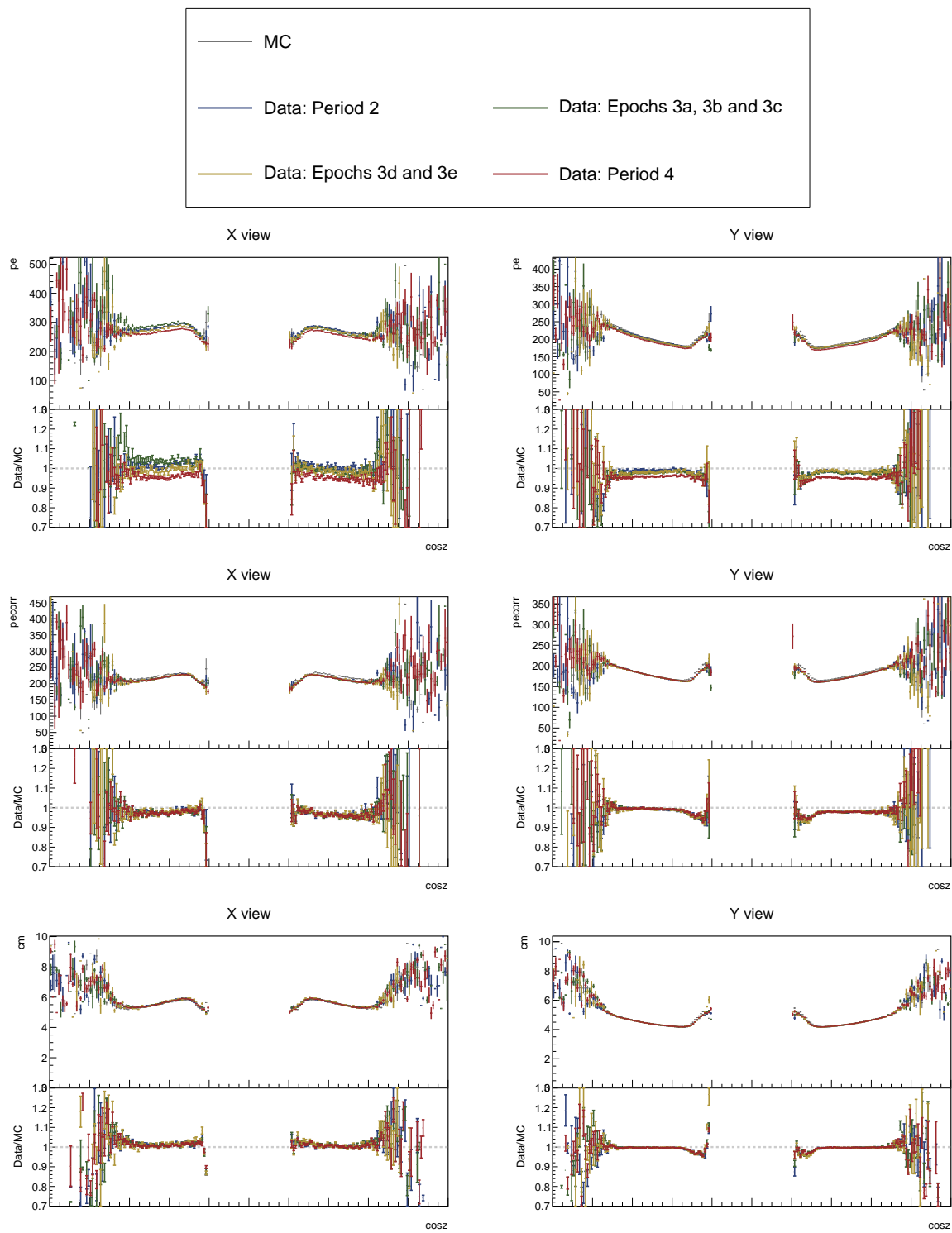


Figure 52: ...

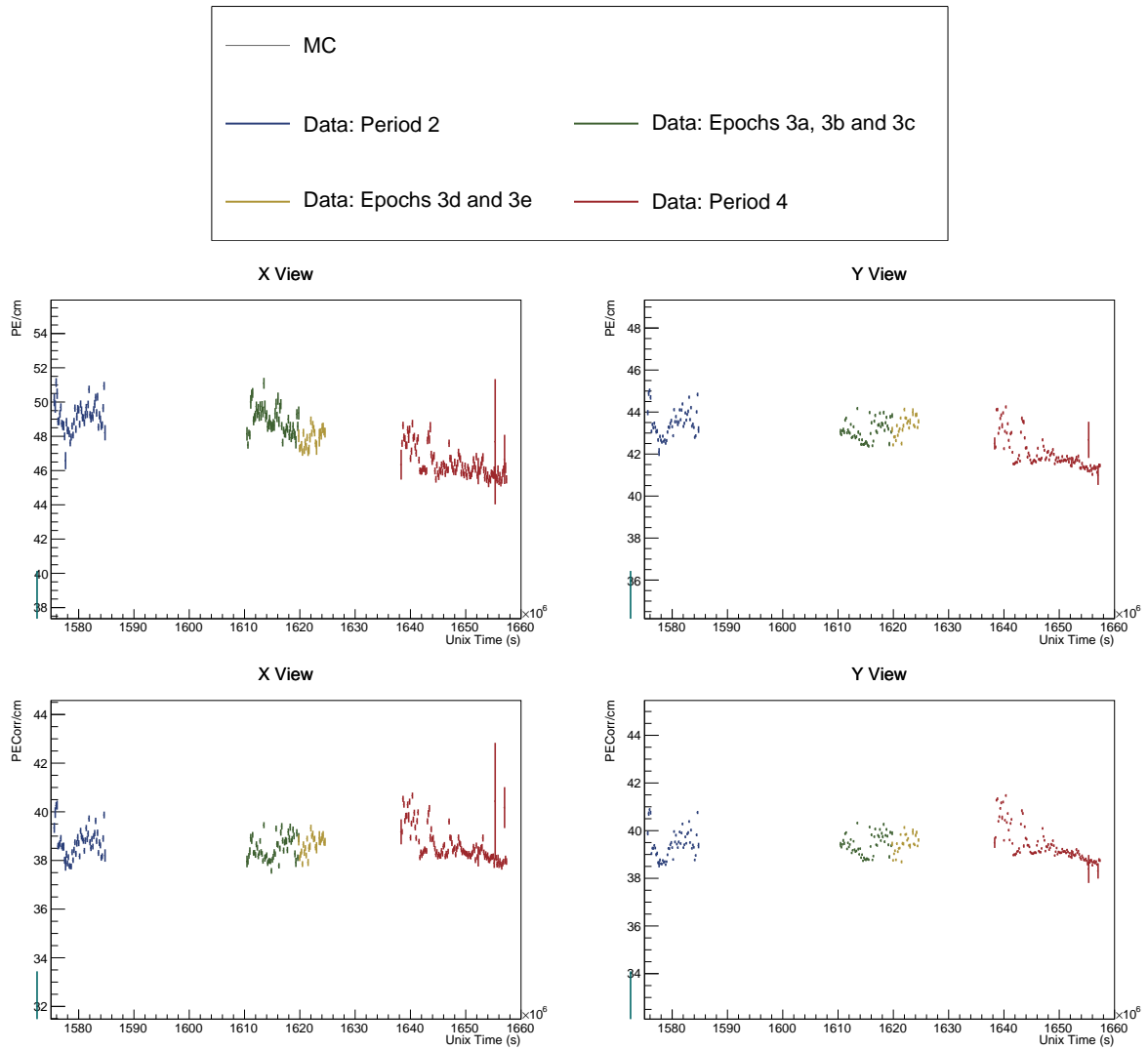


Figure 53: ...

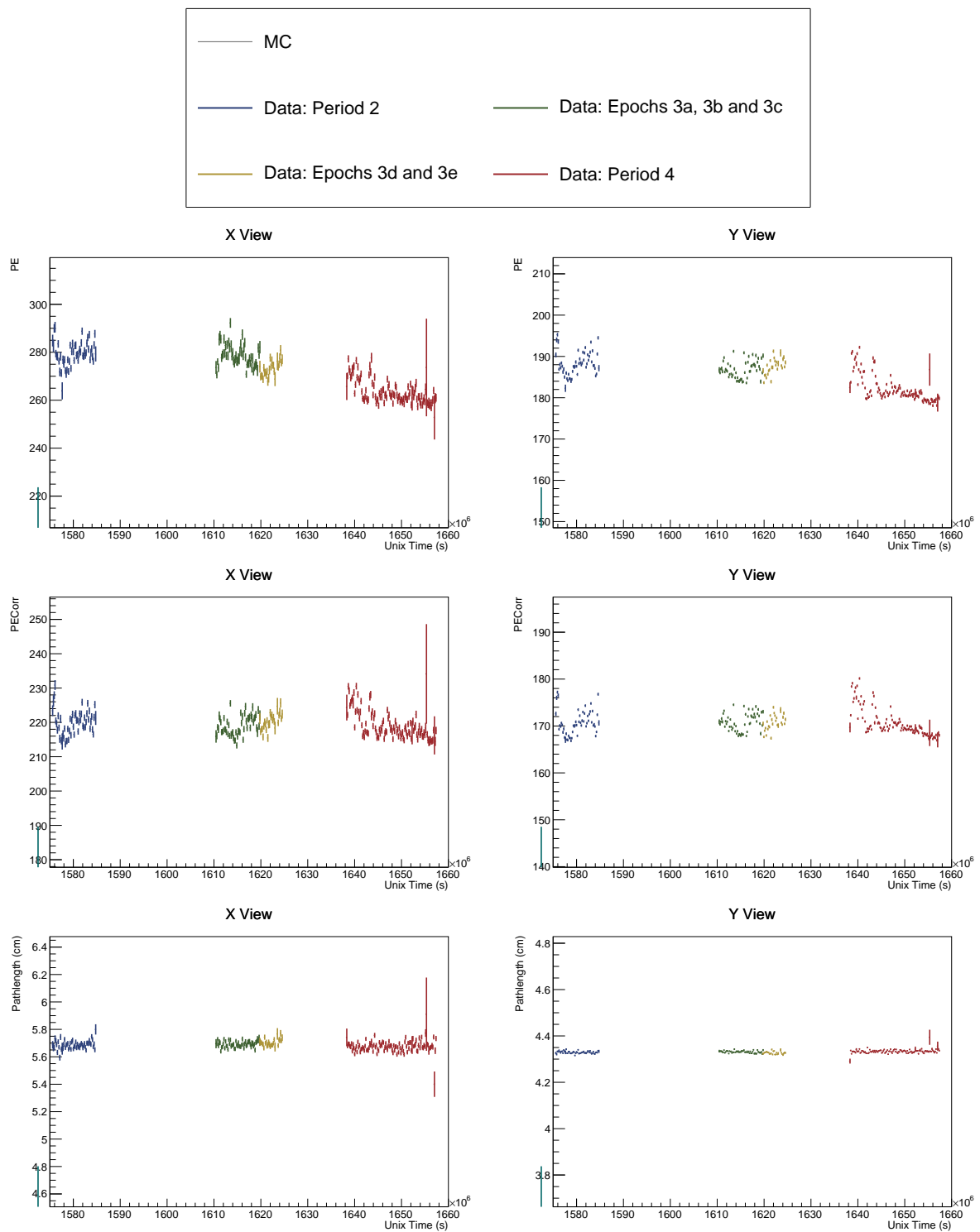


Figure 54: ...

⁴⁶⁶ **5 Conclusion**

⁴⁶⁷ TO DO: Write a conclusion